# Two-Phase Equilibrium and Minimum Miscibility Pressure of $CO_2$-DME-Oil Mixtures

By
Ying Zhou

A thesis submitted in partial fulfillment of the requirements for the degree of

Master of Science

in

Petroleum Engineering

Department of Civil and Environmental Engineering

University of Alberta

## ABSTRACT

$CO_2$ flooding is a widely used enhanced oil recovery (EOR) method (Jarrell *et al*., 2002). Dimethyl ether (DME) is potentially a good solvent and has good compatibility with both $CO_2$ and hydrocarbons (Catchpole *et al*., 2009; Ratnakar *et al*., 2016a). Due to the good solubility of DME in both $CO_2$ and oil, adding DME during $CO_2$ flooding may lower the minimum miscibility pressure (MMP) and enhance the oil recovery efficiency. Therefore, it is necessary to study the phase behavior of $CO_2$-DME-crude oil mixtures. Previous researchers used a constant binary interaction parameter (BIP) between $CO_2$ and DME in Peng-Robinson equation of state (PR EOS) to model the phase equilibrium of $CO_2$-DME mixtures. However, it is found that the BIP between $CO_2$ and DME shows a dependence on temperature. Based on the fitting of two-phase equilibrium data for $CO_2$ and DME mixtures, a linear temperature-dependent BIP correlation for $CO_2$-DME system is firstly obtained. Since no previous researchers focus on the density prediction of $CO_2$-DME system, three volume translation models are applied in PR EOS to improve the vapor-liquid density prediction for $CO_2$-DME mixtures. The predicted results are compared with the experimental data in the literature. It is found that PR EOS with the volume translation model proposed by Abudour *et al*. (2013) provides the most accurate density prediction. In addition, it is essential to determine the minimum miscibility pressure (MMP) during $CO_2$ flooding process. In the second part of the study, the multiple-mixing-cell (MMC) algorithm proposed by Ahmadi and Johns (2011) is adopted for MMP predictions. Prediction results show that adding DME during $CO_2$ flooding can lower the MMP between injection gas and reservoir oil and thus help enhance the oil recovery efficiency.

## DEDICATION

This dissertation is dedicated to my dearest parents: Mrs. Mei Hong and Mr. Kun Zhou.

## ACKNOWLEDGMENTS

I would like to greatly acknowledge my supervisors Dr. Huazhou Li and Dr. Nobuo Maeda for their guidance towards the thesis research and their assistance in preparing the MSc thesis. I am grateful to Dr. Juliana Leung and Dr. Lijun Deng for serving as my examination committee members as well as providing constructive comments and suggestions.

I would also like to thank the following individuals or organizations for their support during my MSc program:

- The past and present group members in Dr. Li and Dr. Maeda's research groups;
- Dr. Ruixue Li at the Chengdu University of Technology for her assistance in programming the Matlab codes;
- All my friends in Edmonton for their friendship.

## TABLE OF CONTENTS

# LIST OF TABLES

## LIST OF FIGURES

# CHAPTER 1 INTRODUCTION

This chapter presents the background of $CO_2$ flooding and phase behavior modeling in $CO_2$ flooding, followed by problem statement, research objectives and thesis outline.

## 1.1.Research Background

### 1.1.1 $CO_2$ Injection for Enhanced Oil Recovery

$CO_2$ flooding has become a widely used enhanced oil recovery (EOR) method over the past years (Jarrell *et al*., 2002) because of its high hydrocarbon recovery efficiency for both light oil and heavy oil (Enick *et al*., 2012) and associated benefit of greenhouse gas emissions reduction (Haszeldine, 2009; Yang *et al*., 2015; Li *et al*., 2016). During the $CO_2$ flooding process, the oil viscosity and the interfacial tension can be both reduced by $CO_2$ injection (Siregar *et al*., 1999; Jaramillo *et al*., 2009). Pressure is an important factor that greatly affects the efficiency of $CO_2$ displacement since its change leads to a substantial change in the in-situ phase behavior of $CO_2$-oil mixtures (Sebastian *et al*., 1985). During $CO_2$ flooding, $CO_2$ becomes miscible with crude oil when the pressure keeps increasing and becomes larger than a threshold pressure level. Miscibility refers to the physical scenario where the constituting substances form one phase at all proportions (Wade, 2013). At a given temperature/pressure condition, if two fluids with all proportions form one phase at first contact, first contact miscibility is reached (Kantzas *et al*., 2012). Multiple contact miscibility is attained when two fluids are immiscible at first contact but form one phase after multiple contacts (Kantzas *et al*., 2012). Miscibility is related to but different from the concept of solubility. Solubility is the maximum quantity of solute that can be dissolved in a certain amount of solvent (Qiu *et al*., 2016). Miscibility between two components is achieved once their mutual solubility reaches 100% (Flowers *et al*., 2018). Miscibility studied in this thesis refers to the

multiple contact miscibility. At MMP, the oil can be extracted effectively due to the fact that reservoir oil and injected $CO_2$ form one phase. The pressure, at which oil can be completely miscible with injected $CO_2$, is called the minimum miscibility pressure (MMP) (Stalkup, 1983). Therefore, it is crucial to obtain precise MMP estimations in $CO_2$ flooding.

Dimethyl ether (DME) is a solvent that can be nearly miscible with hydrocarbons at first contact and partially miscible with water (Cho *et al*., 2018). As it has a relatively high vapor pressure, it can be easily liquefied and be stored in liquefied petroleum gas tanks, which is convenient for transportation (Tallon and Fenton, 2010). These features make it a potential good agent for enhanced $CO_2$ flooding and enhanced waterflooding (Ratnakar *et al*., 2016a). Ratnakar *et al*. (2016a) measured partitioning of DME between hydrocarbons and aqueous phase containing water and salt. The cubic plus association (CPA) model is used in their study to describe the phase equilibrium of DME-water-crude oil system. Then Ratnakar *et al*. (2017) performed more experiments on DME-brine-crude oil system and performed calculations by using Peng-Robinson equation of state (PR EOS) with Huron-Vidal (HV) mixing rule to develop a correlation of DME-partitioning coefficient between oil and brine based on composition of DME in oil phase, temperature, pressure, and salinity of brine (Ratnakar *et al*., 2016b). It showed that the calculation results using the model with the proposed DME-partitioning coefficient correlation match well with the experimental data. Since DME can be dissolved in both hydrocarbons and $CO_2$ (Catchpole *et al*., 2009; Ratnakar *et al*., 2016a), adding DME during $CO_2$ injection process may help reduce the interfacial tension, and reduce the MMP between crude oil and $CO_2$ (Blom *et al*., 2013). In such case, the MMP is governed by the phase behavior of $CO_2$-DME-oil mixtures. It is thus important to have a better understanding of the phase behavior of $CO_2$-DME-oil system in order to capture the effect of DME addition on the MMP.

### 1.1.2 EOS and Volume Translation

Since the first cubic EOS (CEOS) was proposed by van der Waals (1873), many CEOSs, such as PR EOS and Soave-Redlich-Kwong (SRK) EOS, have been introduced to describe the PVT relationship for both pure substances and mixtures (Soave, 1972; Peng and Robinson, 1976). BIP in an EOS represents the relative strength of the intermolecular interactions between like and unlike molecules (Whitson and Brule, 2000). CEOSs are widely used in reservoir simulations due to its computational efficiency (Abudour *et al*., 2012a). Although the CEOS models mentioned above can give a relatively accurate prediction of phase behavior, the accuracy of liquid-phase density prediction needs to be improved (Bell, 2019).

Martin (1979) proposed a new concept called volume translation, which is a transformation of the volume in an EOS by introducing a constant without changing the phase equilibrium, to improve the poor liquid volumetric estimations with CEOSs. Based on Martin's work (1979), Péneloux *et al*. (1982) introduced a constant volume translation parameter, *c*, for improved density calculation with SRK EOS. Péneloux *et al*. (1982) also proved that the volume correction does not change the vapor-liquid phase equilibrium. Inspired by Péneloux *et al*. (1982), Jhaveri and Youngren (1988) combined the constant volume translation model with PR EOS, and the modified PR EOS gives more accurate density predictions than the original PR EOS. Although the density predictions using this model at temperatures away from the reduced temperature $T_r$=0.7 is not as accurate as that at $T_r$=0.7, it is still commonly used today due to its simplicity (Jhaveri and Youngren, 1988; Bell *et al*., 2019). After that, several volume shift models, which are either temperature or density dependent, have been proposed. Ahlers and Gmehling (2001) introduced a temperature dependent volume correction term, which gives good saturated density predictions up to the reduced temperature $T_r$=0.8. Instead of reproducing saturated liquid densities, Baled *et al*. (2012) correlated

the correction term to single-phase density data of pure components at high temperatures and high pressures. Although this model provides very good density predictions under extreme conditions, it fails to give accurate density predictions for light alkanes (Baled *et al*., 2012). The experimental density data of heavy hydrocarbons, which are not easily obtained, are required in correlation process (Baled *et al*., 2012). Frey *et al*. (2009) coupled a new distance function with SRK EOS and later extended the model to mixtures (Frey *et al*., 2013). However, the improvement of density prediction at high temperatures and pressures using this model is not obvious (Liu *et al*., 2010). It was shown by Shi and Li (2016) that some temperature-dependent volume translation models lead to a crossing of isotherms in the pressure-volume (PV) diagram. Later, Shi *et al.* (2018) developed an improved temperature-dependent volume translation model for PR EOS that only yields the crossover of pressure-volume isotherms under high pressure/temperature conditions.

Chou *et al*. (1989) defined a dimensionless distance function for SRK EOS that can be used to well capture the relationship between the needed volume translation and the distance to the critical point of a pure substance. Almost at the same time, Mathias *et al*. (1989) developed a similar distance function for PR EOS. Based on the works by Chou *et al*. (1989) and Mathias *et al*. (1989), Abudour *et al*. (2012a) changed the constant term in the volume shift function to an exponential function, resulting in more accurate density estimations in both saturated and single-phase regions. The volume translation model developed by Abudour *et al*. (2012a) is probably the most accurate volume translation available in the literature, but it is noted that the distance-function-based volume translation model may change the actual phase equilibrium since it is both temperature and pressure dependent.

### 1.1.3 MMP Determination

In order to obtain precise MMPs in $CO_2$ flooding, experimental and computational methods have been developed. Slim-tube test, which considers the phase behavior of reservoir fluid and injection gas, is the most commonly used experimental method for determining MMPs (Yellig and Metcalfe, 1980; Li *et al*., 2012). However, the slim-tube test is expensive and time-consuming, and it may not predict MMP accurately due to the dispersion phenomenon and limited data points (Johns *et al*., 2002). Dispersion phenomenon takes place when a fluid flows through a porous medium, which results in nonuniform fluid velocities (Fried and Combarnous, 1971). For vaporizing or condensing gas drive, multi-contact single-mixing-cell experiments can well describe MMPs accurately (Zick, 1986). However, for miscibility achieved by a combined condensing and vaporizing drive, multi-contact single-mixing-cell experiments cannot provide accurate MMP predictions (Zick, 1986; Johns *et al*., 1993). Slim-tube compositional simulation reproduces the flow of reservoir oil and injection gas in the slim-tube tests (Yellig and Metcalfe, 1980), but one of its drawbacks is the high computational demand (Li and Li, 2019).

Computational methods based on EOS are the mainstream theoretical method for MMP predictions. Three main computational methods (method of characteristics (MOC), slim-tube compositional simulation, and multiple mixing-cell (MMC) method) are used for MMP determination (Ahmadi and Johns, 2011). The analytical MOC method is developed for 1D displacements without dispersion phenomenon (Orr, 2007). Jensen and Michelsen (1990) first proposed the oil tie line and the gas tie line for pure vaporizing drives or condensing drives. In addition to the oil tie line and the gas tie line, the crossover tie line may also control the miscible process (Monroe *et al*., 1990). Orr *et al*. (1993) proved the existence of the crossover tie line in a quaternary mixture and provided a simple method to find it. Johns *et al*. (1993) then presented a

simple geometric construction to determine the crossover tie line for two cases in which the miscibility is achieved via combined condensing and vaporizing gas drive. The oil tie line, the gas tie line, and the crossover tie line are generally called key tie lines (Monroe *et al*., 1990). It was concluded that the key tie line controls the development of miscibility in such combined process (Johns *et al*., 1993). Johns and Orr (1997) presented an algorithm to find the key tie line controlling the development of miscibility. Wang and Orr (1997) extended the analytical method that Johns and Orr (1996) proposed to multicomponent system and later extended the previous work to multicomponent reservoir oils or injection gases (Wang and Orr, 2000). However, Yuan and Johns (2005) pointed out that the MOC algorithm might converge to wrong key tie lines, resulting in false solutions.

Metcalfe *et al*. (1973) first proposed a novel MMC method for the MMP determination in gas injection. It was later modified by Jaubert *et al*. (1998a, b) to enable more pragmatic implementation of this MMC method. The MMC method developed by Jaubert *et al*. (1998a) tries to physically mimic the slim-tube displacement process. Ahmadi and Johns (2011) developed another MMC method whose procedure is fundamentally different from the one proposed by Metcalfe *et al*. (1973). Unlike the aforementioned method, Ahmadi and Johns (2011) proposed a simple but robust MMC method. It does not mimic the physical displacement process, but it can effectively allow for the full development of all key tie lines (Ahmadi and Johns, 2011). At the first contact, the two-phase equilibrium of injection gas and reservoir oil is solved by negative flash calculations with an EOS, providing the compositions of both liquid and vapor phases (Whitson and Michelsen, 1989; Leibovici and Nichita, 2008). As the equilibrium vapor phase moves faster than the equilibrium liquid phase, the vapor phase is mixed with another cell of reservoir oil, while the liquid phase is mixed with another cell of injection gas at the second series

of contact (Ahmadi and Johns, 2011). A series of contacts continue until all the key tie lines are fully developed (Ahmadi and Johns, 2011). The procedure is repeated at different pressures, and the minimum tie line length of all key tie lines at each pressure is recorded (Ahmadi and Johns, 2011). The pressure, where the minimum key tie line length is zero, is regarded as the MMP (Ahmadi and Johns, 2011). Later a robust vapor-liquid-asphaltene three-phase flash code was coupled with the MMC method to predict MMP under the influence of asphaltene precipitation (Li and Li, 2019).

### 1.2. Problem Statement

A reliable thermodynamic model is needed to simulate the phase behaviour of $CO_2$-DME-oil mixtures. On one hand, previous researchers used a constant BIP value between $CO_2$ and DME for the phase equilibria calculations using PR EOS. But phase-equilibrium calculations for $CO_2$-DME mixtures using constant BIPs are not accurate enough. On the other hand, there are no previous works which have focused on the density predictions for $CO_2$-DME mixtures. Besides, no study has examined the effect of adding DME on the MMPs of $CO_2$-oil mixtures.

### 1.3. Research Objectives

The objectives of this research include the following:

- To develop a temperature-dependent function of BIP for $CO_2$-DME mixtures by fitting the experimental vapor-liquid phase equilibria data available in the literature;
- To more accurately predict the density of $CO_2$-DME mixtures using volume translation methods and the regressed temperature-dependent BIPs; and
- To conduct MMC simulations to investigate the effect of adding DME into $CO_2$ stream on the MMP between injection gas and reservoir oil.

### 1.4. Thesis Structure

In this thesis, PR EOS is utilized to model the phase behavior of $CO_2$-DME mixtures. The BIPs between $CO_2$ and DME, which are required in flash calculations, are obtained by regressing the phase equilibria data reported by Tsang and Streett (1981). Density of $CO_2$-DME mixtures predicted with PR EOS and volume translation models is compared with the measured data reported by Tallon and Fenton (2010). The MMC algorithm for MMP determination proposed by Ahmadi and Johns (2011) is employed in order to give good predictions for the MMPs of $CO_2$-DME-oil mixtures; they are then compared with the predicted MMPs of $CO_2$-oil mixtures to examine the effect of DME addition on MMP reduction.

This thesis contains four chapters:

- Chapter 1 introduces the research background, literature review, problem statement, research objectives, and thesis structure.
- Chapter 2 presents the thermodynamic model used for predicting the phase behavior of $CO_2$-DME mixtures and the modeling framework used for MMP determinations.
- Chapter 3 shows the regressed temperature-dependent BIP correlation for $CO_2$-DME mixtures, compares the density calculations using three different models, and presents the effect of adding DME during $CO_2$ flooding on the MMPs between injection gas and reservoir oil.
- Chapter 4 summarizes the conclusions drawn from this thesis work and the recommendations for future work.

**References**

Abudour, A.M., Mohammad, S.A., Robinson Jr, R.L., Gasem, K.A., 2012. Volume-translated Peng-Robinson equation of state for saturated and single-phase liquid densities. Fluid Phase Equilibr. 335, 74-87.

Ahlers, J., Gmehling, J., 2001. Development of an universal group contribution equation of state: I. Prediction of liquid densities for pure compounds with a volume translated Peng-Robinson equation of state. Fluid Phase Equilibr. 191 (1-2), 177-188.

Ahmadi, K., Johns, R.T., 2011. Multiple-mixing-cell method for MMP calculations. SPE J. 16 (04), 733-742.

Baled, H., Enick, R.M., Wu, Y., McHugh, M.A., Burgess, W., Tapriyal, D., Morreale, B.D., 2012. Prediction of hydrocarbon densities at extreme conditions using volume-translated SRK and PR equations of state fit to high temperature, high pressure PVT data. Fluid Phase Equilibr. 317, 65-76.

Bell, I.H., Welliquet, J., Mondejar, M.E., Bazyleva, A., Quoilin, S., Haglind, F., 2019. Application of the group contribution volume translated Peng-Robinson equation of state to new commercial refrigerant mixtures. Int. J. Refrig. 103, 316-328.

Blom, C.P.A., Hedden, R., Matzakos, A.N., Uehara-Nagamine, E., 2013. Oil recovery process, USA Patent US20130161010A1.

Catchpole, O.J., Tallon, S.J., Eltringham, W.E., Grey, J.B., Fenton, K.A., Vagi, E.M., Vyssotski, M.V., MacKenzie, A.N., Ryan, J., Zhu, Y., 2009. The extraction and fractionation of specialty lipids using near critical fluids. J. Supercrit. Fluid. 47 (3), 591-597.

Cho, J., Kim, T.H., Lee, K.S., 2018. Compositional modeling and simulation of dimethyl ether (DME)- enhanced waterflood to investigate oil mobility improvement. Pet. Sci. 15, 297-304.

Chou, G.F., Prausnitz, J.M., 1989. A phenomenological correction to an equation of state for the critical region. AIChE J. 35 (9), 1487-1496.

Enick, R.M., Olsen, D.K., Ammer, J.R., Schuller, W., 2012. Mobility and conformance control for $CO_2$ EOR via thickeners, foams, and gels-A literature review of 40 years of research and pilot tests. SPE 154122.

Flowers, P., Neth, E.J., Theopold, K., Langley, R., Robinson, W.R., 2018. Chemistry: Atoms First. OpenStax and the University of Connecticut and UConn Undergraduate Student Government Association.

Frey, K., Modell, M., Tester, J.W., 2009. Density-and-temperature-dependent volume translation for the SRK EOS: 1. Pure fluids. Fluid Phase Equilibr. 279 (1), 56-63.

Frey, K., Modell, M., Tester, J.W., 2013. Density-and-temperature-dependent volume translation for the SRK EOS: 2. Mixtures. Fluid Phase Equilibr. 343, 13-23.

Fried, J.J., Combarnous, M.A., 1971. Dispersion in porous media (Vol. 7). Elsevier.

Haszeldine, R.S., 2009. Carbon capture and storage: how green can black be? Sci. 325 (5948), 1647-1652.

Jaramillo, P., Griffin, W.M., McCoy, S.T., 2009. Life cycle inventory of $CO_2$ in an enhanced oil recovery system. Environ. Sci. Technol. 43, 8027-8032.

Jarrell, P.M., Fox, C.E., Stein, M.H., Webb, S.L., 2002. Practical aspects of $CO_2$ flooding (Vol. 22). Richardson, TX: Society of Petroleum Engineers.

Jaubert, J.N., Arras, L., Neau, E., Avaullee, L., 1998b. Properly defining the classical vaporizing and condensing mechanisms when a gas is injected into a crude oil. Ind. Eng. Chem. Res. 37 (12), 4860-4869.

Jaubert, J.N., Wolff, L., Neau, E., Avaullee, L., 1998a. A very simple multiple mixing cell calculation to compute the minimum miscibility pressure whatever the displacement mechanism. Ind. Eng. Chem. Res. 37 (12), 4854-4859.

Jensen, F., Michelsen, M.L., 1990. Calculation of first contract and multiple contact minimum miscibility pressures. In Situ. 14 (1), 1-17.

Jhaveri, B.S., Youngren, G.K., 1988. Three-parameter modification of the Peng-Robinson equation of state to improve volumetric predictions. SPE Res. Eng. 3 (03), 1-033.

Johns, R.T., Dindoruk, B., Orr, F.M., 1993. Analytical theory of combined condensing/vaporizing gas drives. SPE Adv. Tech. Ser. 1 (02), 7-16.

Johns, R.T., Orr, F.M., 1996. Miscible gas displacement of multicomponent oils. SPE J. 1 (01), 39-50.

Johns, R.T., Sah, P., Solano, R., 2002. Effect of dispersion on local displacement efficiency for multicomponent enriched-gas floods above the minimum miscibility enrichment. SPE Res. Eval. Eng. 5 (01), 4-10.

Kantzas, A., Bryan, J., Taheri, S., 2012. Fundamentals of Fluid Flow in Porous Media.

Leibovici, C.F., Nichita, D.V., 2008. A new look at multiphase Rachford-Rice equations for negative flashes. Fluid Phase Equilibr. 267 (2), 127-132.

Li, H., Qin, J., Yang, D., 2012. An improved $CO_2$-oil minimum miscibility pressure correlation for live and dead crude oils. Ind. Eng. Chem. Res. 51 (8), 3516-3523.

Li, R., Li, H., 2019. A modified multiple-mixing-cell algorithm for minimum miscibility pressure prediction with the consideration of the asphaltene-precipitation effect. Ind. Eng. Chem. Res. 58 (33), 15332-15343.

Li, S., Li, Z., Dong, Q., 2016. Diffusion coefficients of supercritical $CO_2$ in oil-saturated cores under low permeability reservoir conditions. J. $CO_2$ Util. 14, 47-60.

Liu, K., Wu, Y., McHugh, M.A., Baled, H., Enick, R.M., Morreale, B.D., 2010. Equation of state modeling of high-pressure, high-temperature hydrocarbon density data. J. Supercrit. Fluid. 55 (2), 701-711.

Martin, J.J., 1979. Cubic equations of state-which? Ind. Eng. Chem. Fund. 18 (2), 81-97.

Mathias, P.M., Naheiri, T., Oh, E.M., 1989. A density correction for the Peng-Robinson equation of state. Fluid Phase Equilibr. 47 (1), 77-87.

Metcalfe, R.S., Fussell, D.D., Shelton, J.L., 1973. A multicell equilibrium separation model for the study of multiple contact miscibility in rich-gas drives. SPE J. 13 (03), 147-155.

Monroe, W.W., Silva, M.K., Larson, L.L., Orr, F.M., 1990. Composition paths in four-component systems: effect of dissolved methane on 1D $CO_2$ flood performance. SPE Res. Eng. 5 (03), 423-432.

Orr, F.M., 2007. Theory of gas injection processes (Vol. 5). Copenhagen: Tie-Line Publications.

Orr, F.M., Johns, R.T., Dindoruk, B., 1993. Development of miscibility in four-component $CO_2$ floods. SPE Res. Eng. 8 (02), 135-142.

Pedersen, K.S., Christensen, P.L., Shaikh, J.A., 2014. Phase behavior of petroleum reservoir fluids. CRC press.

Péneloux, A., Rauzy, E., Fréze, R., 1982. A consistent correction for Redlich-Kwong-Soave volumes. Fluid Phase Equilibr. 8 (1), 7-23.

Peng, D.Y., Robinson, D.B., 1976. A new two-constant equation of state. Ind. Eng. Chem. Fund. 15 (1), 59-64.

Qiu, Y., Chen, Y., Zhang, G.G., Yu, L., Mantri, R.V. eds., 2016. Developing solid oral dosage forms: pharmaceutical theory and practice. Academic press.

Ratnakar, R.R., Dindoruk, B., Wilson, L., 2016a. Experimental investigation of DME-water-crude oil phase behavior and PVT modeling for the application of DME-enhanced water flooding. Fuel. 182, 188-197.

Ratnakar, R.R., Dindoruk, B., Wilson, L., 2016b. Use of DME as an EOR agent: experimental and modeling study to capture interactions of DME, brine and crudes at reservoir conditions. SPE 181515.

Ratnakar, R.R., Dindoruk, B., Wilson, L.C., 2017. Phase behavior experiments and PVT modeling of DME-brine-crude oil mixtures based on Huron-Vidal mixing rules for EOR applications. Fluid Phase Equilibr. 434, 49-62.

Sebastian, H. M., Wenger, R. S., Renner, T.A., 1985. Correlation of minimum miscibility pressure for impure $CO_2$ streams. J. Pet. Technol. 37 (11), 2-076.

Shi, J., Li, H.A., 2016. Criterion for determining crossover phenomenon in volume-translated equation of states. Fluid Phase Equilibr. 430, 1-12.

Shi, J., Li, H.A., Pang, W., 2018. An improved volume translation strategy for PR EOS without crossover issue. Fluid Phase Equilibr. 470, 164-175.

Siregar, S., Mardisewojo, P., Kristanto, D., Tjahyadi, R., 1999. Dynamic interaction between $CO_2$ gas and crude oil in porous medium. SPE 57300.

Soave, G., 1972. Equilibrium constants from a modified Redlich-Kwong equation of state. Chem. Eng. Sci. 27 (6), 1197-1203.

Stalkup, F.I., 1983. Miscible Displacement (Vol. 8). NY: Society of Petroleum Engineers of AIME.

Tallon, S., Fenton, K., 2010. The solubility of water in mixtures of dimethyl ether and carbon dioxide. Fluid Phase Equilibr. 298 (1), 60-66.

Tsang, C.Y., Streett, W.B., 1981. Vapor-liquid equilibrium in the system carbon dioxide/dimethyl ether. J. Chem. Eng. Data. 26 (2), 155-159.

van der Waals, J.D., 1873. Continuity of the gaseous and liquid state of matter. University of Leiden.

Wade, L.G., 2013. Organic chemistry: pearson new international edition. Pearson Higher Ed.

Wang, Y., Orr, F.M., 1997. Analytical calculation of minimum miscibility Cure. Fluid Phase Equilibr. 139 (1-2), 101-124.

Wang, Y., Orr, F.M., 2000. Calculation of minimum miscibility pressure. J. Petrol. Sci. Eng. 27 (3-4), 151-164.

Whitson, C.H., Brule, M.R., 2000. Phase Behavior (Vol. 20). SPE Monograph Series.

Whitson, C.H., Michelsen, M.L., 1989. The negative flash. Fluid Phase Equilibr. 53, 51-71.

Yang, Z., Liu, X., Hua, Z., Ling, Y., Li, M., Lin, M., Dong, Z., 2015. Interfacial tension of $CO_2$ and crude oils under high pressure and temperature. Colloids Surf. A Physicochem. Eng. Asp. 482, 611-616.

Yellig, W.F., Metcalfe, R.S., 1980. Determination and prediction of $CO_2$ minimum miscibility pressures (includes associated paper 8876). J. Pet. Technol. 32 (01), 160-168.

Yuan, H., Johns, R.T., 2005. Simplified method for calculation of minimum miscibility pressure or enrichment. SPE J. 10 (04), 416-425.

Zick, A.A., 1986. A combined condensing/vaporizing mechanism in the displacement of oil by enriched gases. SPE 15493.

# CHAPTER 2 MATHEMATICAL FORMULATIONS

This chapter introduces the mathematical formulations of the thermodynamic models used for modeling the phase behavior of $CO_2$-DME-oil mixtures and determining the MMP between injection gas and reservoir oil.

## 2.1. Thermodynamic Model

### 2.1.1 Phase Equilibrium Calculations

#### 2.1.1.1 PR EOS

The phase behavior of the $CO_2$-DME mixture is modeled by applying PR EOS, which is given by (Peng and Robinson, 1976):

$$P = \frac{RT}{v-b} - \frac{a}{v(v+b)+b(v-b)} \quad (1)$$

where $P$ is pressure, $T$ is temperature, $v$ is molar volume, $a$ and $b$ are EOS constants:

$$a = \Omega_a^o \frac{R^2 T_C^2}{p_C} \alpha(T_r, \omega) \quad (2)$$

$$b = \Omega_b^o \frac{RT_C}{P_C} \quad (3)$$

where $P_c$ is critical pressure, $T_c$ is critical temperature, $\alpha$ is a correction term for $a$, $T_r$ is the reduced temperature ($T_r = \frac{T}{T_c}$), $\omega$ is acentric factor, which is defined as description of non-sphericity of molecules (Pitzer, 1955), $\Omega_a^0 = 0.45724$, and $\Omega_b^0 = 0.07780$.

PR EOS can also be expressed in terms of compressibility factor ($Z$) (Peng and Robinson, 1976):

$$Z^3 - (1-B)Z^2 + (A - 3B^2 - 2B)Z - (AB - B^2 - B^3) = 0 \quad (4)$$

$$\mathrm{A} = \frac{aP}{(RT)^2} \text{ (5)}$$

$$B = \frac{bP}{RT} \text{ (6)}$$

The $\alpha$-function is given by (Peng and Robinson, 1976):

$$\alpha = [1 + m(1 - \sqrt{T_r})]^2 \text{ (7)}$$

When $\omega < 0.49$, $m$ is given by (Peng and Robinson, 1976):

$$m = 0.37464 + 1.54226\omega - 0.26992\omega^2 \text{ (8)}$$

and when $\omega > 0.49$, $m$ can be expressed by (Robinson *et al*., 1979; Robinson and Peng, 1978):

$$m = 0.3796 + 1.485\omega - 0.1644\omega^2 + 0.1667\omega^3 \text{ (9)}$$

Mixing rule is used to calculate the EOS parameters *A* and *B* for a given mixture by considering the individual contributions of two substances to these two terms, which eventually enables one to calculate compressibility factor *Z* based on the *A* and *B* terms of the mixture (Whitson and Brule, 2000). In this thesis, van der Waal's mixing rule is adopted for phase equilibrium calculation of mixtures (Peng and Robinson, 1976):

$$A = \sum_{i=1}^{N} \sum_{j=1}^{N} x_i x_j A_{ij} \text{ (10)}$$

$$A_{ij} = \left(1 - k_{ij}\right)\sqrt{A_i A_j} \text{ (11)}$$

$$B = \sum_{i=1}^{N} x_i B_i \text{ (12)}$$

where $k_{ij}$ is the BIP value between component $i$ and $j$, and $x_i$ represents the mole fraction of component $i$, $A_i$, $A_j$ denote EOS constant $A$ of component $i$ and $j$, respectively. $B_i$, $B_j$ denote EOS constant $B$ of component $i$ and $j$, respectively, and $N$ is the number of components.

#### 2.1.1.2 Phase Stability Test

Phase stability test is used to determine whether a phase is stable or not by judging if the Gibbs free energy can be further reduced by splitting the phase into two or more phases at a given temperature and pressure (Whitson and Brule, 2000). It can be implemented before flash calculation to ensure the reliability of flash calculation (Whitson and Brule, 2000). Michelsen (1982a) introduced the tangent plane distance (TPD) function:

$$TPD = \sum_{i=1}^{N} y_i[\ln y_i + \ln \emptyset_i(y) - \ln z_i - \ln \emptyset_i(z)] \quad (13)$$

where $y_i$ represents the trial phase composition, $z_i$ is the feed composition, and $\emptyset_i$ is the fugacity coefficient of each component. The given system can be considered thermodynamically stable as a single phase when the TPD values calculated at all feed compositions are equal to or greater than zero (Michelson, 1982a). On the contrary, the given mixture can be regarded as unstable if the TPD values are smaller than zero (Michelson, 1982a). Michelsen (1982a) also suggested that only TPD values at the stationary points should be calculated instead of all TPD values. The TPD function at stationary points is given by (Michelsen, 1982a):

$$\ln y_i + \ln \emptyset_i(y) - \ln z_i - \ln \emptyset_i(z) = K \quad (14)$$

where $K$ is a constant. The equation (14) can be simplified by introducing new variables $Y_i = \exp(-K)y_i$ (Michelsen, 1982a):

$$\ln Y_i + \ln \emptyset_i(Y) - \ln z_i - \ln \emptyset_i(z) = 0 \quad (15)$$

Also, the TPD expression can be rewritten in the term of $Y_i$ as below (Michelsen, 1982a):

$$TPD = 1 + \sum_{i=1}^{N} Y_i[ln\varphi_i(Y) + lnY_i - ln\varphi_i(z) - lnz_i - 1] \quad (16)$$

#### 2.1.1.3 Two-phase Vapor-liquid Flash Calculations

A mathematical method for solving two-phase flash was proposed by Michelson (1982a, b). Material-balance constraint and equal-fugacity constraint need to be satisfied in this approach. A typical two-phase flash algorithm has two loops: the outer loop updates the equilibrium ratios, while the inner loop solves the Rachford-Rice (RR) equation (Michelsen, 1982a, b; Rachford and Rice, 1952). $K_i$ is defined as the equilibrium ratio, which can be calculated as:

$$K_i = \frac{y_i}{x_i} \quad (17)$$

$K_i$ can be initialized by the application of the Wilson equation (Wilson, 1969):

$$K_i = \frac{\exp[5.37(1+\omega_i)(1-T_{ri}^{-1})]}{P_{ri}} \quad (18)$$

where $\omega_i$ is the acentric factor of component $i$, $T_{ri}$ represents the reduced temperature of component $i$, and $P_{ri}$ represents the reduced pressure of component $i$. With the equilibrium ratio fed into the inner loop, the vapor mole fraction can be solved using the RR equation (Rachford and Rice, 1952). The RR equation is given as (Rachford and Rice, 1952):

$$h(F_v) = \sum_{i=1}^{N}(y_i - x_i) = \sum_{i=1}^{N} \frac{z_i(K_i-1)}{1+F_v(K_i-1)} = 0 \quad (19)$$

where $F_v$ denotes the vapor mole fraction, $x_i$ and $y_i$ are the mole fractions of each component in the liquid phase and the vapor phase, respectively. Then the phase compositions in both liquid and vapor phase can be updated using equations below (Michelson, 1982b):

$$x_i = \frac{z_i}{F_v(K_i-1)+1} \quad (20)$$

$$y_i = \frac{z_i K_i}{F_v(K_i-1)+1} = K_i x_i \quad (21)$$

With the phase compositions known, the EOS constants *A* and *B* can be obtained using equations (10) and (12). Then the *Z* factor for each phase can be calculated by solving equation (4). Eventually, fugacity for each phase can be calculated by (Peng and Robinson, 1976):

$$\ln\frac{f_i}{x_i p} = \frac{B_i}{B}(Z-1) - \ln(Z-B) + \frac{A}{2\sqrt{2}B}\left(\frac{B_i}{B} - \frac{2}{A}\sum_{j=1}^{N} y_i A_{ij}\right)\ln\left[\frac{Z+(1+\sqrt{2})B}{Z+(1-\sqrt{2})B}\right] \quad (22)$$

The equation used to update *K* values in the outer loop is given by (Whitson and Brule, 2000):

$$K_i^{(n+1)} = K_i^n \frac{f_{Li}^n}{f_{vi}^n} \quad (23)$$

where $f_{Li}^n$ and $f_{vi}^n$ represent the fugacity values of component $i$ in the liquid phase and vapor phase, respectively, and *n* is the iteration index.

### 2.1.2 Density Prediction Models for Pure Fluids

#### 2.1.2.1 Density Prediction Using PR EOS

Density of a pure substance for each phase is given by:

$$\rho = \frac{MW}{v} \quad (24)$$

where $\rho$, $MW$ and $v$ are density, molecular weight, and molar volume, respectively. The molar volume, $v$, for each phase can be obtained by the real gas equation as given below (Standing, 1977):

$$Pv = ZRT \quad (25)$$

where $R$ is gas constant, and the compressibility factor, $Z$, can be obtained by solving equation (4).

#### 2.1.2.2 Density Prediction Using PR EOS with Constant Volume Translation Model

Jhaveri and Youngren (1988) coupled PR EOS with the constant volume translation model for density prediction. Compared with densities calculated without volume translation, the accuracy of density calculations using their method is improved (Jhaveri and Youngren, 1988). The molar volume can be calculated by (Jhaveri and Youngren, 1988):

$$v = v^{PR} - c_0 \quad (26)$$

where $v$ is corrected molar volume, $v^{PR}$ is the molar volume calculated by PR EOS without volume translation, and $c_0$ is the volume translation term which is assumed to be a constant for a specific substance in this model. The corrected density of each phase can be calculated as soon as the corrected molar volume is obtained. The expression for $c_0$ is given by (Jaubert *et al*., 2016):

$$c_i = \frac{RT_c}{P_c}(0.1154 - 0.4406Z_c) \quad (27)$$

where $Z_{RA}$ is the Rackett compressibility factor, which can be replaced by $Z_c$ value if there is no available $Z_{RA}$ (Spencer and Danner, 1972).

#### 2.1.2.3 Density Prediction Using PR EOS with Abudour *et al.* (2012a) Volume Translation Model

Chou and Prausnitz (1989) defined a dimensionless distance function to characterize the "distance" between a state point and the critical point. The distance function is calculated as per (Chou and Prausnitz, 1989):

$$d^{PR} = \frac{1}{RT_c}\left(\frac{\partial P^{PR}}{\partial \rho^{PR}}\right)_T = \frac{{v^{PR}}^2}{RT_c}\left[\frac{RT}{(v^{PR}-b^{PR})^2} - \frac{2a^{PR}(v^{PR}+b^{PR})}{\left({v^{PR}}^2+2b^{PR}v^{PR}-{b^{PR}}^2\right)^2}\right] \quad (28)$$

where $d^{PR}$ and $\rho^{PR}$ are the dimensionless distance parameter and molar density calculated by the original PR EOS, $a^{PR}$ and $b^{PR}$ are PR EOS constants for a given component. The revised volume translation function by Abudour *et al*. (2012a) takes the following form:

$$v^{VTPR} = v^{PR} + c - \delta_c^{PR}\left(\frac{0.35}{0.35+d^{PR}}\right) \quad (29)$$

where $v^{VTPR}$ is the corrected molar volume, $\delta_c^{PR}$ is the volume shift at the critical temperature, which is given by (Chou and Prausnitz, 1989):

$$\delta_c^{PR} = \frac{RT_c}{P_c}(Z_c^{PR} - Z_c) = v_c^{PR} - v_c \quad (30)$$

where $Z_c^{PR}$ is the critical compressibility factor given by the original PR EOS (i.e., 0.3074), $Z_c$ is the experimental critical compressibility factor, $v_c^{PR}$ and $v_c$ are the theoretical and experimental critical molar volumes, respectively.

Abudour *et al*. (2012a) developed a new *c* function:

$$c = \left(\frac{RT_c}{P_c}\right)(c_1 - (0.004 + c_1)\exp(-2d^{PR})) \quad (31)$$

where $c_1$ is a substance-dependent constant given by (Abudour *et al*., 2012a):

$$c_1 = 0.4266Z_c - 0.1101 \quad (32)$$

### 2.1.3 Mixing Rule

#### 2.1.3.1 Mixing Rule Used in PR EOS

Density of a mixture can be calculated by:

$$\rho_m = \frac{MW_m}{v_m} \quad (33)$$

where $\rho_m$, $MW_m$, and $v_m$ are the density, the molecular weight, and the molar volume of the mixture, respectively. The molecular weight of the mixture can be calculated by:

$$MW_m = \sum_{i=1}^{N} x_i MW_i \quad (34)$$

The molar volume of the mixture can be then obtained by (Standing, 1977):

$$Pv_m = ZRT \quad (35)$$

#### 2.1.3.2 Mixing Rule Used in Constant Volume Translation Model

The molar volume correction term for a mixture, $c_{0_m}$, can be calculated as a mole-fraction average, which is given by (Jhaveri and Youngren, 1988):

$$c_{0_m} = \sum_{i=1}^{N} x_i c_{0_i} \quad (36)$$

where $c_{0_i}$ is the volume translation correction constant of component *i*, and the corrected molar volume, $v_m$, of the mixture for each phase can be calculated by (Jhaveri and Youngren, 1988):

$$v_m = v_m^{PR} - c_{0_m} \quad (37)$$

where $v_m^{PR}$ is the molar volume of the mixture calculated by PR EOS without volume translation.

#### 2.1.3.3 Mixing Rule Used in Abudour *et al.* (2012) Volume Translation Model

The volume translation model proposed by Abudour *et al*. (2012a) was later extended to mixtures by adopting an appropriate mixing rule (Abudour *et al*., 2013). The corrected molar volume for mixtures is given by (Abudour *et al*., 2013):

$$v_m^{VTPR} = v_m^{PR} + c_m - \delta_{cm}^{PR}\left(\frac{0.35}{0.35 + d_m^{PR}}\right) \quad (38)$$

where $v_m^{VTPR}$ is the molar volume of mixtures calculated by the volume-translated PR EOS model, $c_m$ is the volume translation term for mixtures, $\delta_{cm}^{PR}$ is the volume correction at the critical temperature for mixtures, $d_m^{PR}$, which is defined by Chou and Prausnitz (1989), is the dimensionless distance function for mixtures. The equations of $c_m$, $d_m^{PR}$, and $\delta_m^{PR}$ are presented below (Chou and Prausnitz, 1989; Abudour *et al*., 2013):

$$c_m = \left(\frac{RT_{c_m}}{P_{c_m}}\right)\left(c_{1_m} - (0.004 + c_{1_m})\exp(-2d_m^{PR})\right) \quad (39)$$

$$d_m^{PR} = \frac{1}{RT_{c_m}}\left(\frac{\partial P^{PR}}{\partial \rho_m^{PR}}\right)_T = \frac{v_m^{PR^2}}{RT_{c_m}}\left[\frac{RT}{\left(v_m^{PR} - b_m^{PR}\right)^2} - \frac{2a_m^{PR}\left(v_m^{PR} + b_m^{PR}\right)}{\left(v_m^{PR^2} + 2b_m^{PR}v_m^{PR} - b_m^{PR^2}\right)^2}\right] \quad (40)$$

$$\delta_{c_m}^{PR} = \frac{RT_{c_m}}{P_{c_m}}\left(Z_c^{PR} - Z_{c_m}\right) = v_{c_m}^{PR} - v_{c_m} \quad (41)$$

where $T_{c_m}$ and $P_{c_m}$ represent the critical temperature and the critical pressure of mixtures, respectively, $c_{1_m}$ is the component-dependent parameter for mixtures, $v_{c_m}$ is the experimental critical volume of mixtures, $\rho_m^{PR}$ is the molar density of mixtures, $a_m^{PR}$ and $b_m^{PR}$ are EOS constants for mixtures , $Z_{c_m}$ is the experimental critical compressibility factor of mixtures, $v_{c_m}^{PR}$ is the critical volume of mixtures predicted by PR EOS without volume translation. $v_{c_m}^{PR}$ is calculated by (Abudour *et al*., 2013):

$$v_{c_m}^{PR} = \frac{RT_{c_m}}{P_{c_m}} Z_c^{PR} \quad (42)$$

The expression for $c_{1_m}$ appearing in equation (39) is given by (Péneloux et al., 1982):

$$c_{1_m} = \sum_{i=1}^{N} x_i c_{1_i} \quad (43)$$

where $c_{1_i}$ is the $c_1$ value of component $i$. Chueh and Prausnitz (1976) proposed equation (44) for $v_{c_m}$ calculation:

$$v_{c_m} = \sum_{i=1}^{N} \theta_i v_{c_i} \quad (44)$$

where $v_{c_i}$ is the critical molar volume of component $i$, and $\theta_i$ is the surface fraction of component $i$ defined as (Chueh and Prausnitz, 1967):

$$\theta_i = \frac{x_i v_{c_i}^{2/3}}{\sum_{i=1}^{N} x_i v_{c_i}^{2/3}} \quad (45)$$

The critical temperature of mixtures can be calculated by (Chueh and Prausnitz, 1967):

$$T_{c_m} = \sum_{i=1}^{N} \theta_i T_{c_i} \quad (46)$$

where $T_{c_i}$ is the critical temperature for component $i$. The critical pressure of mixtures can be calculated by (Aalto *et al*., 1996):

$$P_{c_m} = \frac{(0.2905 - 0.085\omega_m)RT_{c_m}}{v_{c_m}} \quad (47)$$

where $\omega_m$ is the acentric factor of mixtures (Abudour *et al*., 2013):

$$\omega_m = \sum_{i=1}^{N} x_i \omega_i \quad (48)$$

where $\omega_i$ is the acentric factor of component *i*.

### 2.2. MMC Algorithm for MMP Calculations

The MMC method for MMP calculations proposed by Ahmadi and Johns (2011) is adopted in this study due to its simplicity, robustness and accuracy. The schematic of this algorithm is presented

in Figure 2-1. The procedure of the MMC algorithm is briefly described as follows (Ahmadi and Johns, 2011):

(1) The procedure starts from cells (i.e., an upstream cell and a downstream cell) which are filled with injection gas and reservoir oil, respectively. These cells are under the reservoir temperature. The calculations are firstly conducted as a pressure lower than MMP.

(2) At the first contact, the injection gas is mixed with the reservoir oil with an appropriate mixing ratio. The resulting overall composition of the mixture is given by (Ahmadi and Johns, 2011):

$$z_i = x_i^O + \alpha(y_i^G - x_i^O) \quad (49)$$

where $x_i^O$ and $y_i^G$ are the mole fraction of component *i* in the reservoir oil and the injection gas, respectively, $z_i$ is the mole fraction of component *i* in the resulting mixture, and $\alpha$ denotes the mole fraction of gas phase. Ahmadi and Johns (2011) mentioned that the value of $\alpha$ does not seem to influence the predicted MMPs. They recommend a value of 0.5; this value is used in this study as well.

(3) Negative two-phase vapor-liquid flash calculations using PR EOS are performed (Whitson and Michelsen, 1989; Leibovici and Nichita, 2008). Then phase equilibrium compositions are obtained. The tie line length between the equilibrium liquid phase and equilibrium vapor phase, *TL*, is calculated by (Ahmadi and Johns, 2011):

$$\boldsymbol{TL} = \sqrt{\sum_{\boldsymbol{i=1}}^{\boldsymbol{N}} (\boldsymbol{x_i} - \boldsymbol{y_i})^{\boldsymbol{2}}} \quad (50)$$

where $\boldsymbol{x_i}$ and $\boldsymbol{y_i}$ represent the mole fraction of component *i* in the liquid phase and the vapor phase, respectively.

(4) With the assumption that the equilibrium vapor moves ahead of equilibrium liquid, the vapor phase mixes with fresh reservoir oil, while the equilibrium liquid phase is mixed with another cell of injection gas. Following the same procedure in Step (2) and (3), new equilibrium compositions in each of the contacts are obtained. The aforementioned process is the second contact.

(5) Additional contacts between the neighboring cells continue until all *N*-1 key tie lines are found. A key tie line develops if the tie lines among any three neighboring cells are the same.

(6) The tie line lengths of all key tie lines, which are found in step (5), are calculated. The minimum key tie line length is recorded.

(7) Steps (1) to (6) are repeated at different pressures. Then the plot of the minimum key tie line length versus pressure can be obtained. The MMP can be predicted by the power-law extrapolation of the minimum key tie line lengths obtained at the last several pressures. The power-law extrapolation function is expressed as (Ahmadi and Johns, 2011):

$$\boldsymbol{TL^n = aP + b} \quad (51)$$

where $P$ is pressure, $n$ denotes the optimal exponent, $a$ and $b$ represent the slope and the intercept of the linear equation. The values of $n$, $a$, and $b$ are determined by ensuring the correlation coefficient is larger than 0.999. The predicted MMP value is considered to be the intercept of the above equation at the $x$ axis.

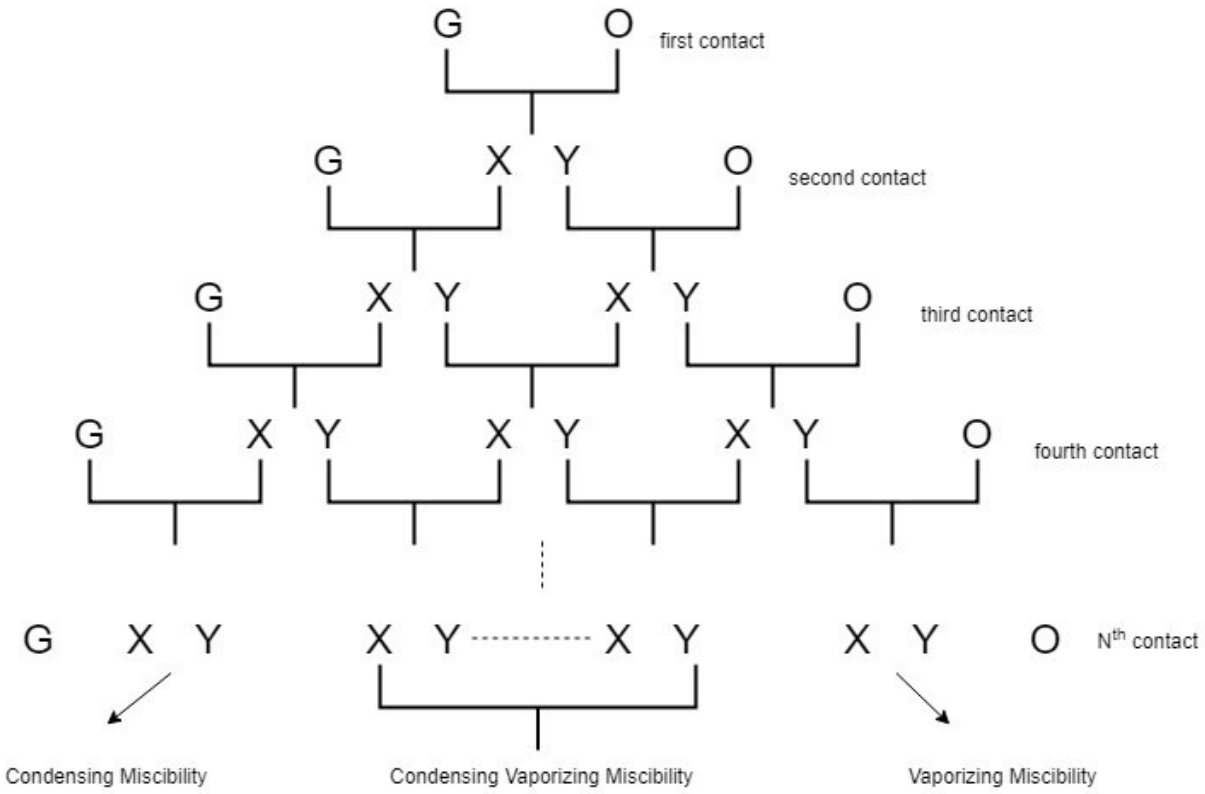


**Figure 2-1** Schematic of the contact method adopted by the MMC method. G: composition of injection gas; O: composition of reservoir oil; X: equilibrium liquid composition; Y: equilibrium gas composition (Adapted from Ahmadi and Johns, 2011).

## References


Aalto, M., Keskinen, K.I., Aittamaa, J., Liukkonen, S., 1996. An improved correlation for compressed liquid densities of hydrocarbons. Part 2. Mixtures. Fluid Phase Equilibr. 114 (1-2), 21-35.

Abudour, A.M., Mohammad, S.A., Robinson Jr, R.L., Gasem, K.A., 2012. Volume-translated Peng-Robinson equation of state for saturated and single-phase liquid densities. Fluid Phase Equilibr. 335, 74-87.

Abudour, A.M., Mohammad, S.A., Robinson Jr, R.L., Gasem, K.A., 2013. Volume-translated Peng-Robinson equation of state for liquid densities of diverse binary mixtures. Fluid Phase Equilibr. 349, 37-55.

Ahmadi, K., Johns, R.T., 2011. Multiple-mixing-cell method for MMP calculations. SPE J. 16 (04), 733-742.

Chou, G.F., Prausnitz, J.M., 1989. A phenomenological correction to an equation of state for the critical region. AIChE J. 35 (9), 1487-1496.

Chueh, P.L., Prausnitz, J.M., 1967. Vapor-liquid equilibria at high pressures: calculation of critical temperatures, volumes, and pressures of nonpolar mixtures. AIChE J. 13 (6), 1107-1113.

Jaubert, J.N., Privat, R., Le Guennec, Y., Coniglio, L., 2016. Note on the properties altered by application of a Péneloux-type volume translation to an equation of state. Fluid Phase Equilibr. 419, 88-95.

Jhaveri, B.S., Youngren, G.K., 1988. Three-parameter modification of the Peng-Robinson equation of state to improve volumetric predictions. SPE Res. Eng. 3 (03), 1-033.

Leibovici, C.F., Nichita, D.V., 2008. A new look at multiphase Rachford-Rice equations for negative flashes. Fluid Phase Equilibr. 267 (2), 127-132.

Michelsen, M.L., 1982a. The isothermal flash problem. Part I. Stability. Fluid Phase Equilibr. 9 (1), 1-19.

Michelsen, M.L., 1982b. The isothermal flash problem. Part II. Phase-split calculation. Fluid Phase Equilibr. 9 (1), 21-40.

Péneloux, A., Rauzy, E., Fréze, R., 1982. A consistent correction for Redlich-Kwong-Soave volumes. Fluid Phase Equilibr. 8 (1), 7-23.

Peng, D.Y., Robinson, D.B., 1976. A new two-constant equation of state. Ind. Eng. Chem. Fund. 15 (1), 59-64.

Pitzer, K.S., 1955. The volumetric and thermodynamic properties of fluids. I. Theoretical basis and virial coefficients. J. Am. Chem. Soc. 77 (13), 3427-3433.

Rachford, H.H., Rice, J.D., 1952. Procedure to use electrical digital computers in calculating flash vaporization hydrocarbon equilibrium. AIME Pet. Trans. 195, 327-328.

Robinson, D.B., Peng, D.Y., 1978. The characterization of the heptanes and heavier fractions. Reasearch Report. 28.

Robinson, D., Peng, D., Ng, H., 1979. Capabilities of the Peng-Robinson programs. 2. 3-phase and hydrate calculations. Hydro. Proc. 58 (9), 269-273.

Spencer, C.F., Danner, R.P., 1972. Improved equation for prediction of saturated liquid density. J. Chem. Eng. Data. 17 (2), 236-241.

Standing, M.B., 1977. Volumetric and phase behavior of oil field hydrocarbon systems. Society of Petroleum Engineers of AIME.

Whitson, C.H., Brule, M.R., 2000. Phase Behavior (Vol. 20). SPE Monograph Series.

Whitson, C.H., Michelsen, M.L., 1989. The negative flash. Fluid Phase Equilibr. 53, 51-71.

Wilson, G.M., 1969. A modified Redlich-Kwong equation of state, application to general physical data calculations. In: 65th National AIChE Meeting, Cleveland, OH.

# CHAPTER 3 RESULTS AND DISCUSSION

In this chapter, a temperature-dependent BIP correlation is calibrated by matching the phase behavior data measured for $CO_2$-DME mixtures. The correlation is then coupled with PR EOS and MMC method to study the effect of adding DME to $CO_2$ on the MMP.

## 3.1. Development of Temperature-dependent BIP Correlation for $CO_2$-DME Binary

### 3.1.1 Experimental Phase Equilibria Data for $CO_2$-DME Mixtures in the Literature

To determine BIPs for the $CO_2$-DME mixture, an experimental database needs to be established. Only very limited experimental works have been made available to measure the phase equilibria of $CO_2$-DME mixtures. In this work, the vapor-liquid composition measurements for $CO_2$-DME system conducted by Tsang and Streett (1981) are employed. In Tsang and Streett's (1981) experiments, the mole fractions of $CO_2$ and DME at equilibrium in each phase were measured at different temperatures ranging from 273.15 K to 386.56 K, and pressures up to 57 bar. The critical properties of $CO_2$ and DME used in the flash calculations are given in Table 3-1. The experimental vapor-liquid equilibrium (VLE) data are presented in Table 3-2. Note that NDP in Table 3-1 denotes the number of data points.

**Table 3-1** Properties of $CO_2$ and DME.

| Component | $T_c$ (K)[a] | $P_c$ (bar)[a] | $\omega$[a] | $MW$ (g/mol)[b] | $Z_c$[b] |
|---|---|---|---|---|---|
| $CO_2$ | 304.2 | 73.83 | 0.239 | 44.01 | 0.274 |
| DME | 400.05 | 52.924 | 0.2 | 46.07 | 0.2744 |

[a] These data are retrieved from Tallon and Fenton (2010).
[b] These data are retrieved from DIPPR.

**Table 3-2** Experimental VLE of $CO_2$-DME system (Tsang and Streett, 1981).

| Temperature (K) | Pressure range (bar) | Mole fraction of $CO_2$ in liquid phase | Mole fraction of $CO_2$ in vapor phase | NDP |
|---|---|---|---|---|
| 273.15 | 2.6-31 | 0.0309-0.9149 | 0.2221-0.9833 | 18 |
| 288.20 | 4.9-44.1 | 0.0169-0.8928 | 0.1937-0.9490 | 16 |
| 308.65 | 8.5-62.6 | 0.0206-0.8611 | 0.1354-0.9329 | 20 |
| 320.06 | 11.4-72.5 | 0.0201-0.8242 | 0.0864-0.8825 | 19 |
| 335.17 | 17.9-79.3 | 0.0448-0.7364 | 0.1563-0.7701 | 12 |
| 350.20 | 21.7-73.9 | 0.0112-0.5795 | 0.0340-0.6263 | 17 |
| 360.07 | 26.1-71.1 | 0.0104-0.4734 | 0.0313-0.5283 | 15 |
| 370.13 | 31.9-66.1 | 0.0134-0.3460 | 0.0317-0.4276 | 16 |
| 377.57 | 35.9-63.7 | 0.0101-0.2765 | 0.0187-0.3288 | 12 |
| 386.56 | 41.9-57 | 0.0060-0.1417 | 0.0102-0.1744 | 9 |

### 3.1.2 Data Reduction Method

The optimized BIP for $CO_2$-DME system at each temperature is acquired by fitting the data in Table 3-2. The objective functions used in the BIP fitting are given by equations (52), (53), and (54). The following objective function, which aims to minimize the deviations between calculation results and experimental data, is used in the BIP fitting if only liquid-phase compositions are available:

$$SS = \sum_{i=1}^{NDP} \sum_{j=1}^{n} \left| \frac{x_{exp} - x_{cal}}{x_{exp}} \right|_i \quad (52)$$

where $SS$ represents the objective function, $n$ denotes the number of components, $x_{exp}$ and $x_{cal}$ are the experimental and calculated liquid mole fractions, respectively. The following objective function is used in the BIP fitting if only vapor-phase compositions are available:

$$SS = \sum_{i=1}^{NDP} \sum_{j=1}^{n} \left| \frac{y_{exp} - y_{cal}}{y_{exp}} \right|_i \quad (53)$$

where $y_{exp}$ and $y_{cal}$ are the experimental and calculated vapor mole fractions, respectively. Lastly, the following objective function can be applied if both liquid-phase and vapor-phase compositions are available:

$$SS = \sum_{i=1}^{NDP} \sum_{j=1}^{n} \left[ \left| \frac{x_{exp} - x_{cal}}{x_{exp}} \right|_i + \left| \frac{y_{exp} - y_{cal}}{y_{exp}} \right|_i \right] \quad (54)$$

### 3.1.3 Temperature-dependent BIP Correlation for $CO_2$-DME Binary

When optimizing a given BIP value at a given temperature, two-phase flash calculations are carried out at different pressures to find out the compositions of the vapor phase and/or liquid phase; the outputted compositions of vapor phase and/or liquid phase are then used to evaluate the objective functions given above. The BIP value that minimizes the objective functions is found to be optimum BIP at that given temperature. Linear regression is utilized to model the relationship between the optimized BIPs and temperature in this thesis. The regression results are analyzed in the terms of the average absolute percentage deviations (%AAD) as below (Abudour *et al*., 2012b):

$$\%AAD = \frac{100}{NDP} \sum_{i=1}^{NDP} \left| \frac{x_{exp} - x_{cal}}{x_{exp}} \right|_i \quad (55)$$

A temperature-dependent correlation of BIP for $CO_2$-DME mixtures can be regressed (see Figure 3-1). The correlation is given as:

$$k_{ij} = 0.000231T - 0.092450 \quad (56)$$

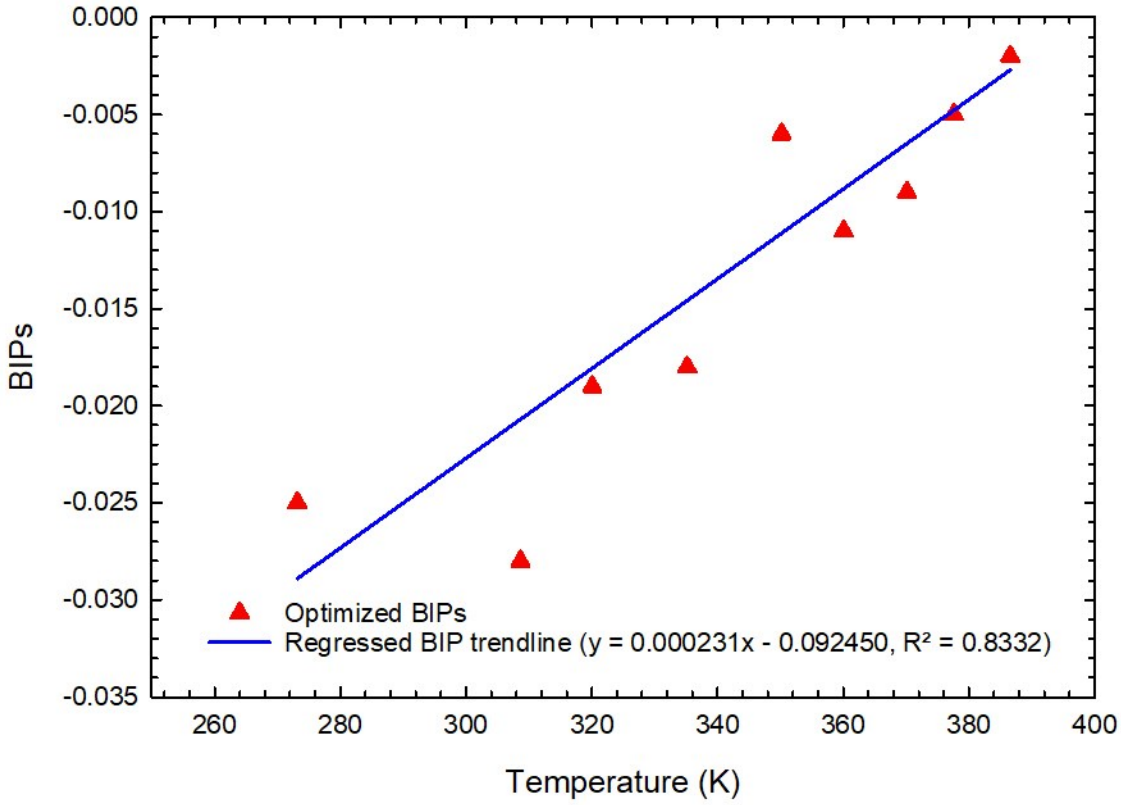


**Figure 3-1** Optimized BIPs at different temperatures and its linear approximation.

Figure 3-2 compares the measured pressure-composition (*P-x*) phase diagrams for $CO_2$-DME binary (Tsang and Streett, 1981) against those calculated using PR EOS together with the BIP correlation. It can be seen from Figure 3-2 that the calculation results match well with the experimental data. Figure 3-3 provides a detailed comparison of the measured VLE composition data and calculated ones using the BIP correlation. Again Figure 3-3 demonstrates an excellent agreement between the calculated mole fractions of $CO_2$ and DME and measured ones. Tallon and Fenton (2010) applied PR EOS to perform phase calculations for $CO_2$-DME binary, and the regressed BIP value between $CO_2$ and DME in their study is -0.049 (Tallon and Fenton, 2010). The deviations between the calculated results with different BIPs and the experimental data are

listed in Table 3-3. It shows that the %AAD provided by using PR EOS with the BIP correlation is much lower than that obtained using PR EOS with the constant BIP of -0.049. For example, at 377.57 K, the BIP correlation improves the VLE composition calculations by reducing 5.95%AAD (obtained with the constant BIP) to 1.48%AAD. PR EOS with the BIP correlation at 370.13 K yields an error of 1.69%AAD, which is significantly lower than the counterpart error of 5.56%AAD. The average %AAD of VLE compositions at 335.17 K is reduced from 6.17 obtained by PR EOS with the constant BIP of -0.049 to 2.14 calculated by PR EOS with the BIP correlation. The overall %AAD in reproducing VLE compositions yielded by PR EOS with the BIP correlation is 3.04, which is lower than 6.73%AAD yielded by PR EOS with the constant BIP of -0.049. Table 3-4 presents the comparison between the %AADs in reproducing the mole fractions of each component in each phase using PR EOS with the BIP correlation and those obtained using the constant BIP of -0.049. Again, it shows that the %AAD generated by the temperature-dependent BIP correlation is smaller than the ones yielded by the constant BIP of -0.049. By using the BIP correlation, the overall %AAD in reproducing the mole fraction of $CO_2$ in liquid phase is reduced from 8.57 to 3.19. The overall %AAD in reproducing the mole fraction of DME in liquid phase yielded by PR EOS with the BIP correlation is 1.04, which is lower than 3.37%AAD yielded by PR EOS with the constant BIP of -0.049. When the BIP correlation is used, the overall %AAD in reproducing the mole fraction of $CO_2$ in vapor phase is reduced from 5.99 to 3.15, while the overall %AAD in reproducing the mole fraction of DME in vapor phase is reduced from 8.98 to 4.78. It can be concluded that PR EOS with the regressed BIP correlation in this thesis gives much more accurate reproduction of VLE compositions than PR EOS with the constant BIP.

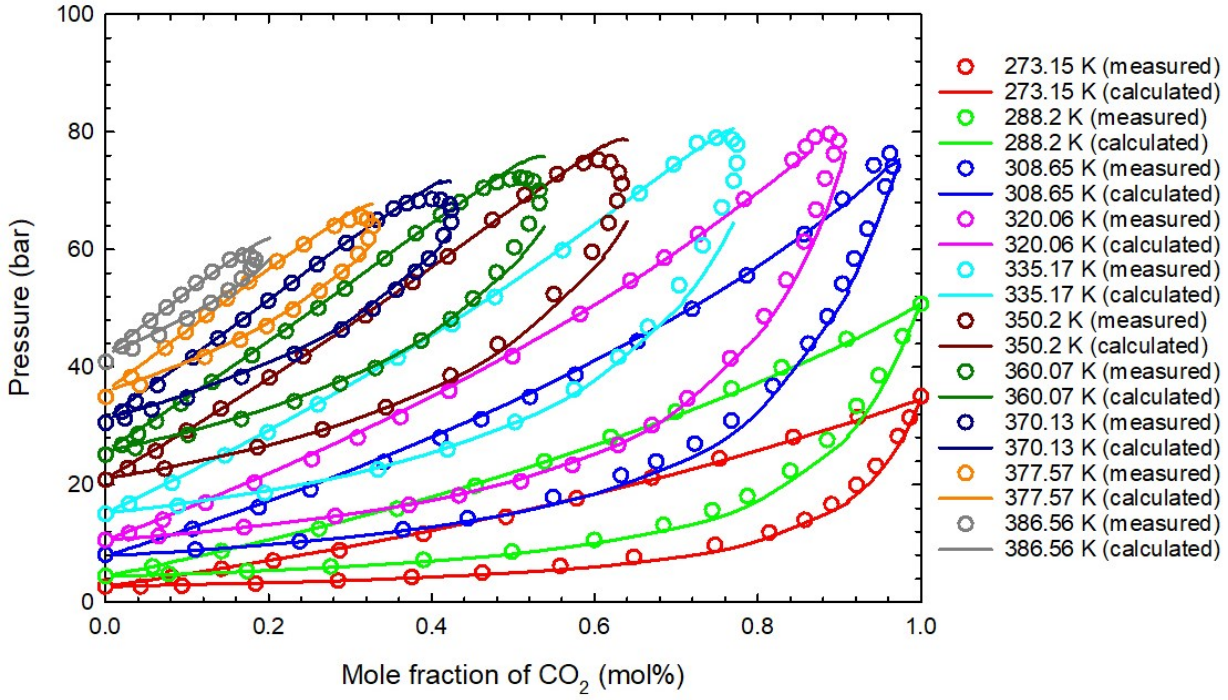


**Figure 3-2** Comparison of *P-x* phase diagrams calculated using the temperature-dependent BIP correlation and measured ones (Tsang and Streett, 1981).

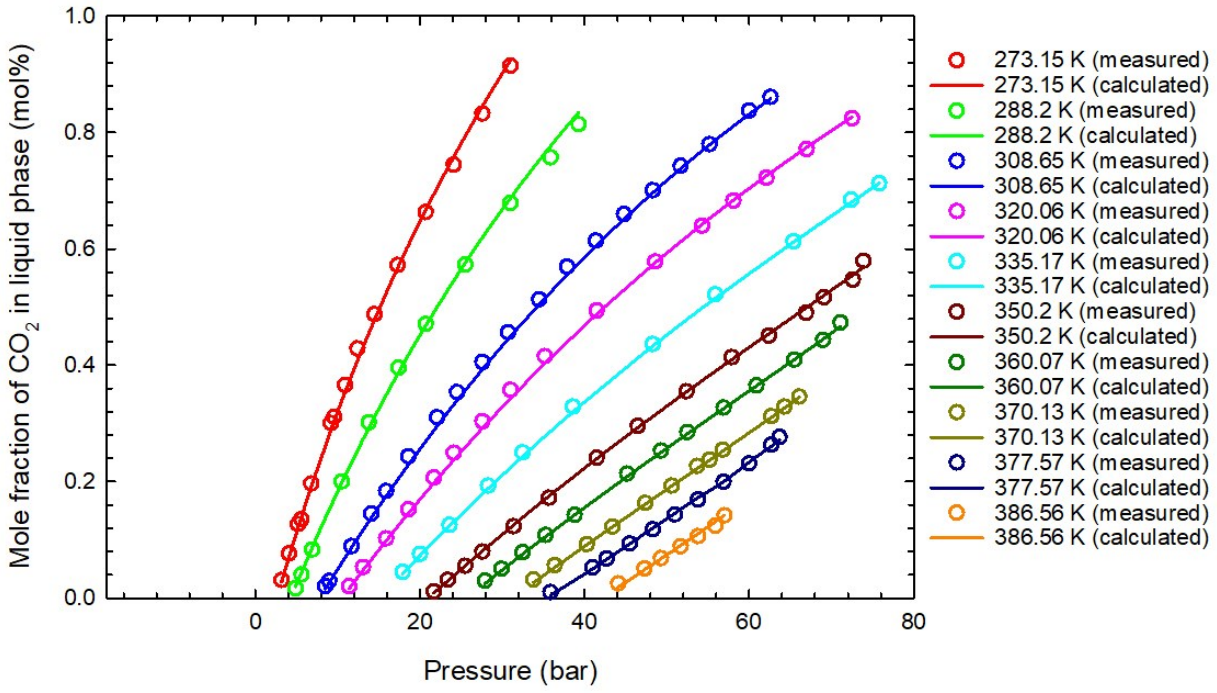
Mole fraction of $CO_2$ in liquid phase (mol%)
Pressure (bar)
0.0
0.2
0.4
0.6
0.8
1.0
0
20
40
60
80
273.15 K (measured)
273.15 K (calculated)
288.2 K (measured)
288.2 K (calculated)
308.65 K (measured)
308.65 K (calculated)
320.06 K (measured)
320.06 K (calculated)
335.17 K (measured)
335.17 K (calculated)
350.2 K (measured)
350.2 K (calculated)
360.07 K (measured)
360.07 K (calculated)
370.13 K (measured)
370.13 K (calculated)
377.57 K (measured)
377.57 K (calculated)
386.56 K (measured)
386.56 K (calculated)

(a)

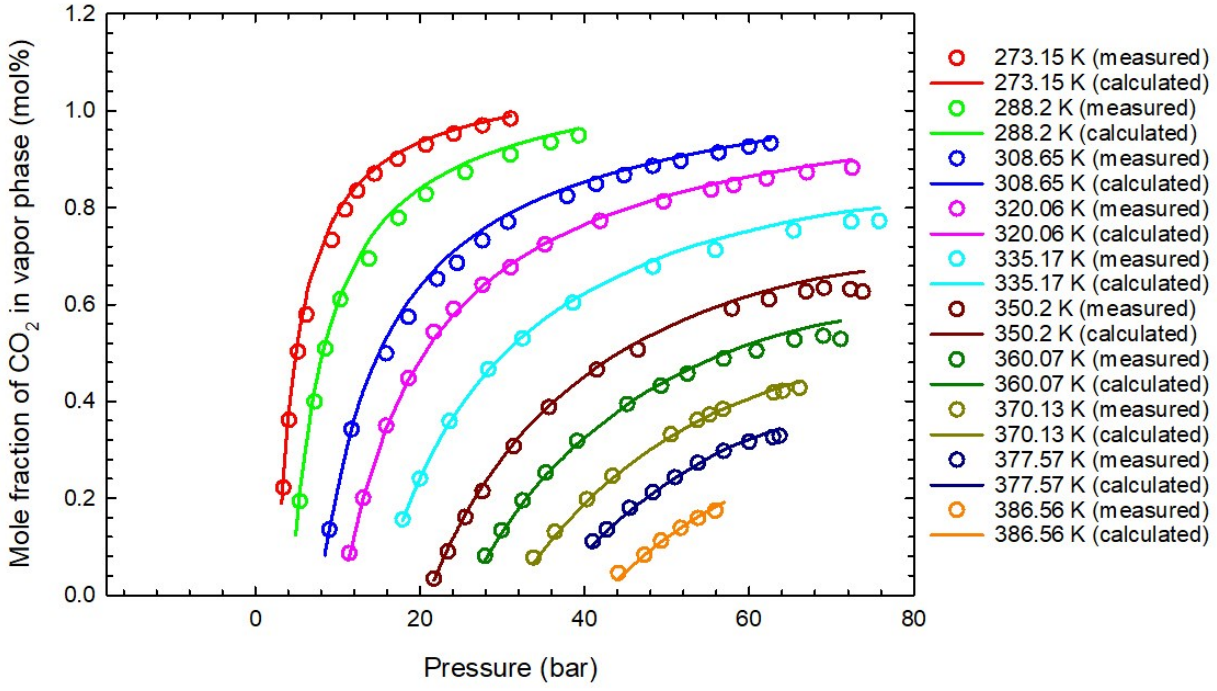
Mole fraction of $CO_2$ in vapor phase (mol%)
Pressure (bar)
0.0
0.2
0.4
0.6
0.8
1.0
1.2
0
20
40
60
80
273.15 K (measured)
273.15 K (calculated)
288.2 K (measured)
288.2 K (calculated)
308.65 K (measured)
308.65 K (calculated)
320.06 K (measured)
320.06 K (calculated)
335.17 K (measured)
335.17 K (calculated)
350.2 K (measured)
350.2 K (calculated)
360.07 K (measured)
360.07 K (calculated)
370.13 K (measured)
370.13 K (calculated)
377.57 K (measured)
377.57 K (calculated)
386.56 K (measured)
386.56 K (calculated)

(b)

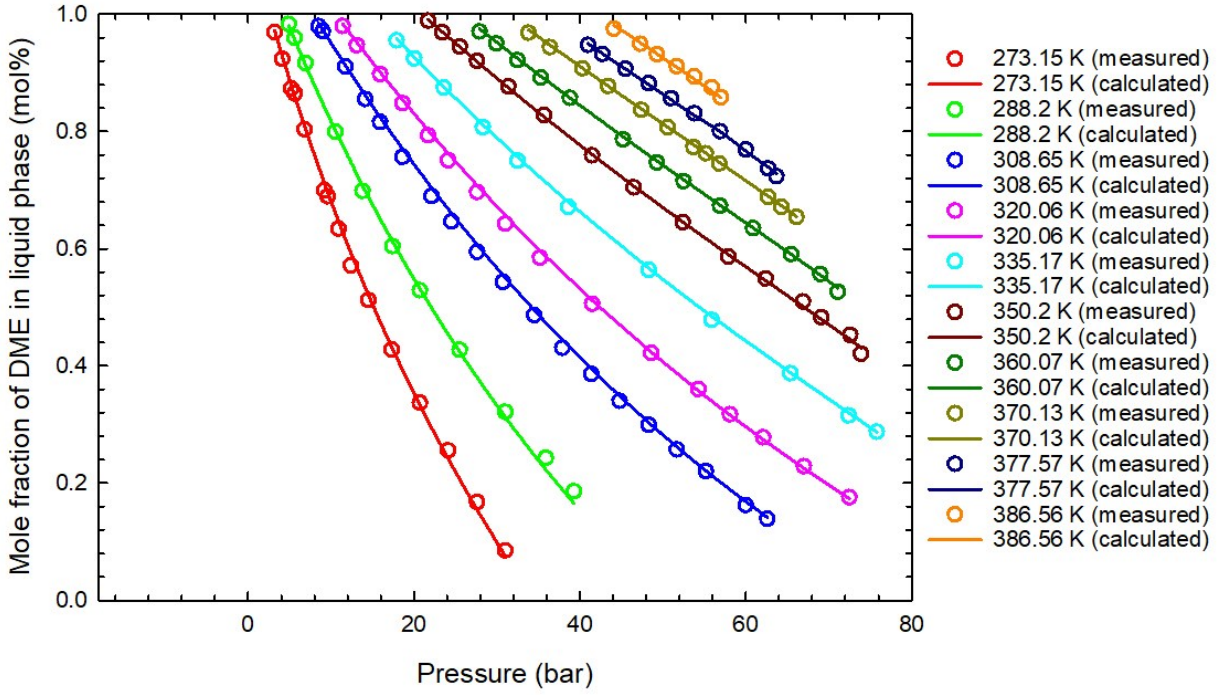


(c)

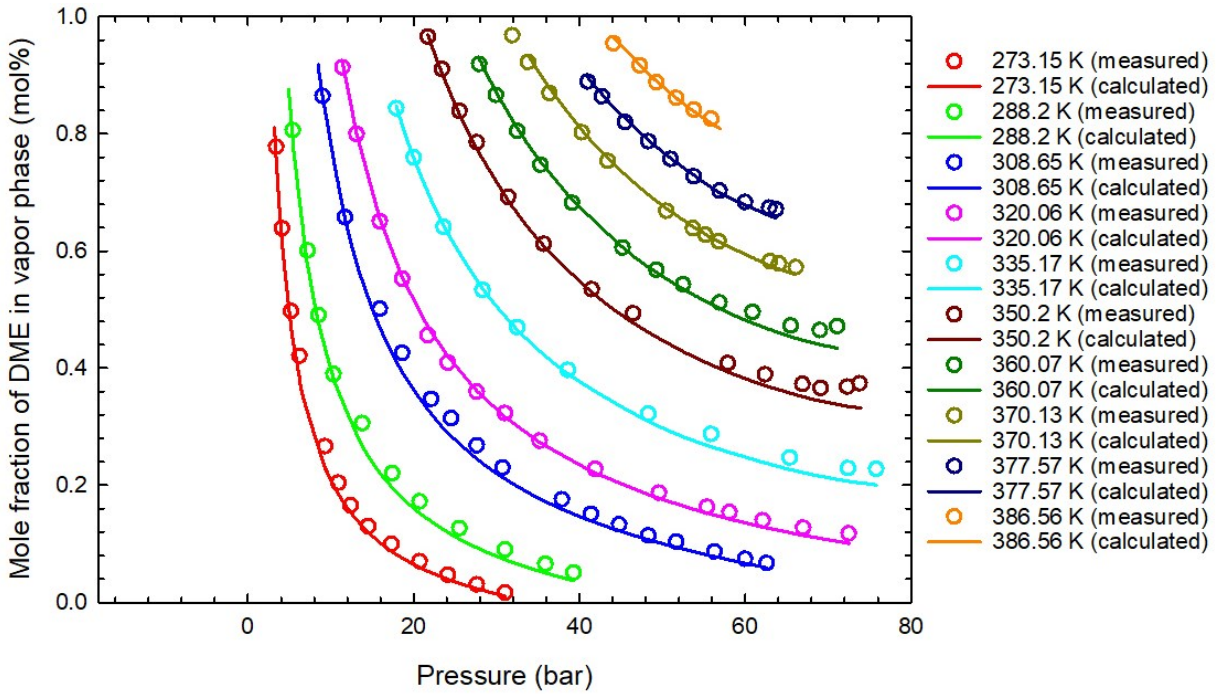


(d)

**Figure 3-3** Comparison of measured VLE composition data and calculated ones using the temperature-dependent BIP correlation: (a) Mole fraction of $CO_2$ in liquid phase; (b) Mole fraction of $CO_2$ in vapor phase; (c) Mole fraction of DME in liquid phase; (d) Mole fraction of DME in vapor phase.

**Table 3-3** Comparison between the deviations yielded by the temperature-dependent BIP correlation and that yielded by the constant BIP.

| Temperature (K) | Average AAD% in reproducing liquid and vapor phase compositions | |
|---|---|---|
| | PR EOS with the temperature-dependent BIP correlation | PR EOS with the constant BIP (-0.049)[a] |
| 273.15 | 5.32 | 7.93 |
| 288.20 | 5.36 | 9.40 |
| 308.65 | 3.82 | 6.73 |
| 320.06 | 2.62 | 5.41 |
| 335.17 | 2.14 | 6.17 |
| 350.20 | 2.73 | 7.52 |
| 360.07 | 2.22 | 5.83 |
| 370.13 | 1.69 | 5.56 |
| 377.57 | 1.48 | 5.95 |
| 386.56 | 3.03 | 6.79 |
| Overall %AAD | 3.04 | 6.73 |

[a] The BIP value is retrieved from Tallon and Fenton (2010).

**Table 3-4** %AAD in reproducing VLE compositions calculated by PR EOS with the temperature-dependent BIP correlation and the constant BIP.

| *T* (K) | %AAD in reproducing phase compositions | | | | | | | |
|---|---|---|---|---|---|---|---|---|
| | Mole fraction of $CO_2$ in liquid phase | | Mole fraction of DME in liquid phase | | Mole fraction of $CO_2$ in vapor phase | | Mole fraction of DME in vapor phase | |
| | PR EOS with the BIP correlation | PR EOS with constant BIP (-0.049)[a] | PR EOS with the BIP correlation | PR EOS with constant BIP (-0.049)[a] | PR EOS with the BIP correlation | PR EOS with constant BIP (-0.049)[a] | PR EOS with the BIP correlation | PR EOS with constant BIP (-0.049)[a] |
| 273.15 | 3.25 | 4.92 | 2.62 | 4.29 | 3.14 | 4.30 | 12.26 | 18.22 |
| 288.20 | 3.82 | 9.43 | 2.45 | 6.02 | 3.33 | 5.09 | 11.84 | 17.08 |
| 308.65 | 3.84 | 4.27 | 1.71 | 2.94 | 2.23 | 4.16 | 7.48 | 15.54 |
| 320.06 | 3.57 | 5.38 | 1.08 | 3.81 | 1.73 | 2.99 | 4.10 | 9.45 |
| 335.17 | 1.99 | 7.55 | 0.67 | 3.59 | 1.76 | 4.64 | 4.13 | 8.91 |
| 350.20 | 2.61 | 10.30 | 0.66 | 3.90 | 4.11 | 8.08 | 3.53 | 7.78 |
| 360.07 | 2.68 | 8.75 | 0.36 | 3.01 | 3.59 | 6.25 | 2.26 | 5.30 |
| 370.13 | 2.45 | 9.56 | 0.25 | 2.72 | 3.18 | 6.44 | 0.89 | 3.53 |
| 377.57 | 1.73 | 11.98 | 0.29 | 2.32 | 3.01 | 6.78 | 0.89 | 2.74 |
| 386.56 | 5.91 | 13.60 | 0.35 | 1.11 | 5.43 | 11.19 | 0.45 | 1.26 |
| Overall %AAD | 3.19 | 8.57 | 1.04 | 3.37 | 3.15 | 5.99 | 4.78 | 8.98 |

[a] The BIP value is retrieved from Tallon and Fenton (2010).

### 3.1.4 VLE Density Predictions

In this part, three different density calculation models (i.e. PR EOS without volume translation, PR EOS with the constant volume translation model proposed by Jhaveri and Youngren (1988), and PR EOS with the volume translation model proposed by Abudour *et al*. (2013)) are applied to calculate the densities of $CO_2$-DME mixtures at different temperatures and pressures. The temperature-dependent BIP correlation is applied during this process to show the effect of using the optimized BIPs as inputs on the calculations of densities. The properties of $CO_2$ and DME used in density calculations are listed in Table 3-1. The calculated densities are then compared with the experimental data measured by Tallon and Fenton (2010). Calculated densities using the aforementioned three models are listed in Table 3-5 and shown in Figure 3-4. It can be seen from Table 3-5 and Figure 3-4 that the %AAD of the density prediction for $CO_2$-DME mixtures with PR EOS is reduced from 4.10 to 3.23 by using the temperature-dependent BIP correlation. As for PR EOS with the constant volume translation model proposed by Jhaveri and Youngren (1988), the %AAD produced by the temperature-dependent BIP correlation is 3.22, which is lower compared with 4.09%AAD generated by the constant BIP (-0.049). When PR EOS with the volume translation model proposed by Abudour *et al*. (2013) is applied to $CO_2$-DME mixtures, the temperature-dependent BIP correlation yields 0.57%AAD, lower than 1.18%AAD that is yielded by the constant BIP (-0.049). It can be concluded that the temperature-dependent BIP correlation developed in this thesis does not only improve the accuracy of predicting VLE compositions, but also improve the accuracy of VLE density predictions for $CO_2$-DME mixtures. Among the aforementioned three density prediction models, PR EOS with the volume translation model proposed by Abudour *et al*. (2013) can provide the most accurate density predictions for $CO_2$-DME mixtures.

**Table 3-5** Comparison of predicted VLE density for $CO_2$-DME binary using different density prediction models.

| *P* (bar) | *T* (K) | Measured density (kg/m$^3$)[a] | Feed composition | | Predicted density (kg/m$^3$) | | | | | |
|---|---|---|---|---|---|---|---|---|---|---|
| | | | | | PR EOS without volume translation | | PR EOS with the constant volume translation model proposed by Jhaveri and Youngren (1988) | | PR EOS with the volume translation model proposed by Abudour *et al*. (2013) | |
| | | | $CO_2$ | DME | With the BIP correlation | With the constant BIP (-0.049)[a] | With the BIP correlation | With the constant BIP (-0.049)[a] | With the temperature-dependent BIP correlation | With the constant BIP (-0.049)[a] |
| 41 | 290.2 | 806 | 0.749 | 0.251 | 817.27 | 828.07 | 817.19 | 827.99 | 816.98 | 824.60 |
| 51 | 292.2 | 805 | | | 815.16 | 825.94 | 815.08 | 825.86 | 814.33 | 822.04 |
| 61 | 292.1 | 811 | | | 824.89 | 835.01 | 824.81 | 834.92 | 820.54 | 827.94 |
| 71 | 292.1 | 817 | | | 833.37 | 842.99 | 833.29 | 842.9 | 826.08 | 833.23 |
| 81 | 292.0 | 824 | | | 841.77 | 850.91 | 841.69 | 850.83 | 831.77 | 838.67 |
| 92 | 292.0 | 829 | | | 849.92 | 858.60 | 849.84 | 858.51 | 837.36 | 843.99 |
| 101 | 291.9 | 834 | | | 856.64 | 864.95 | 856.55 | 864.86 | 842.09 | 848.50 |
| 152 | 291.9 | 857 | | | 887.08 | 894.06 | 886.98 | 893.97 | 864.13 | 869.67 |
| 202 | 291.9 | 875 | | | 911.18 | 917.26 | 911.08 | 917.16 | 882.22 | 887.11 |
| 252 | 291.8 | 892 | | | 931.80 | 937.15 | 931.7 | 937.05 | 898.01 | 902.34 |
| 301 | 290.7 | 908 | | | 952.18 | 956.71 | 952.07 | 956.6 | 913.96 | 917.65 |
| 40 | 292.5 | 769 | 0.542 | 0.458 | 787.72 | 795.53 | 787.64 | 795.45 | 770.20 | 776.06 |
| 52 | 292.5 | 773 | | | 794.53 | 801.89 | 794.45 | 801.81 | 774.93 | 780.52 |
| 61 | 292.6 | 776 | | | 798.92 | 806.11 | 798.84 | 806.03 | 778.00 | 783.49 |
| 71 | 292.7 | 780 | | | 803.67 | 810.60 | 803.59 | 810.52 | 781.35 | 786.69 |
| 82 | 292.8 | 783 | | | 808.60 | 816.17 | 808.52 | 816.09 | 784.88 | 790.70 |
| 92 | 293.0 | 786 | | | 812.92 | 819.15 | 812.84 | 819.07 | 787.97 | 792.83 |
| 102 | 293.1 | 789 | | | 816.80 | 823.25 | 816.72 | 823.17 | 790.79 | 795.82 |
| 152 | 293.2 | 804 | | | 836.44 | 841.93 | 836.35 | 841.84 | 805.37 | 809.71 |
| 202 | 293.4 | 817 | | | 852.75 | 857.61 | 852.66 | 857.52 | 817.70 | 821.58 |
| 253 | 293.5 | 830 | | | 867.40 | 871.82 | 867.31 | 871.73 | 828.92 | 832.47 |
| 293 | 293.7 | 839 | | | 877.37 | 881.46 | 877.28 | 881.36 | 836.62 | 839.91 |
| 300 | 293.7 | 840 | | | 879.10 | 883.16 | 879.01 | 883.07 | 837.96 | 841.23 |
| | | | | %AAD | 3.23 | 4.10 | 3.22 | 4.09 | 0.57 | 1.18 |

[a] These data are retrieved from Tallon and Fenton (2010).

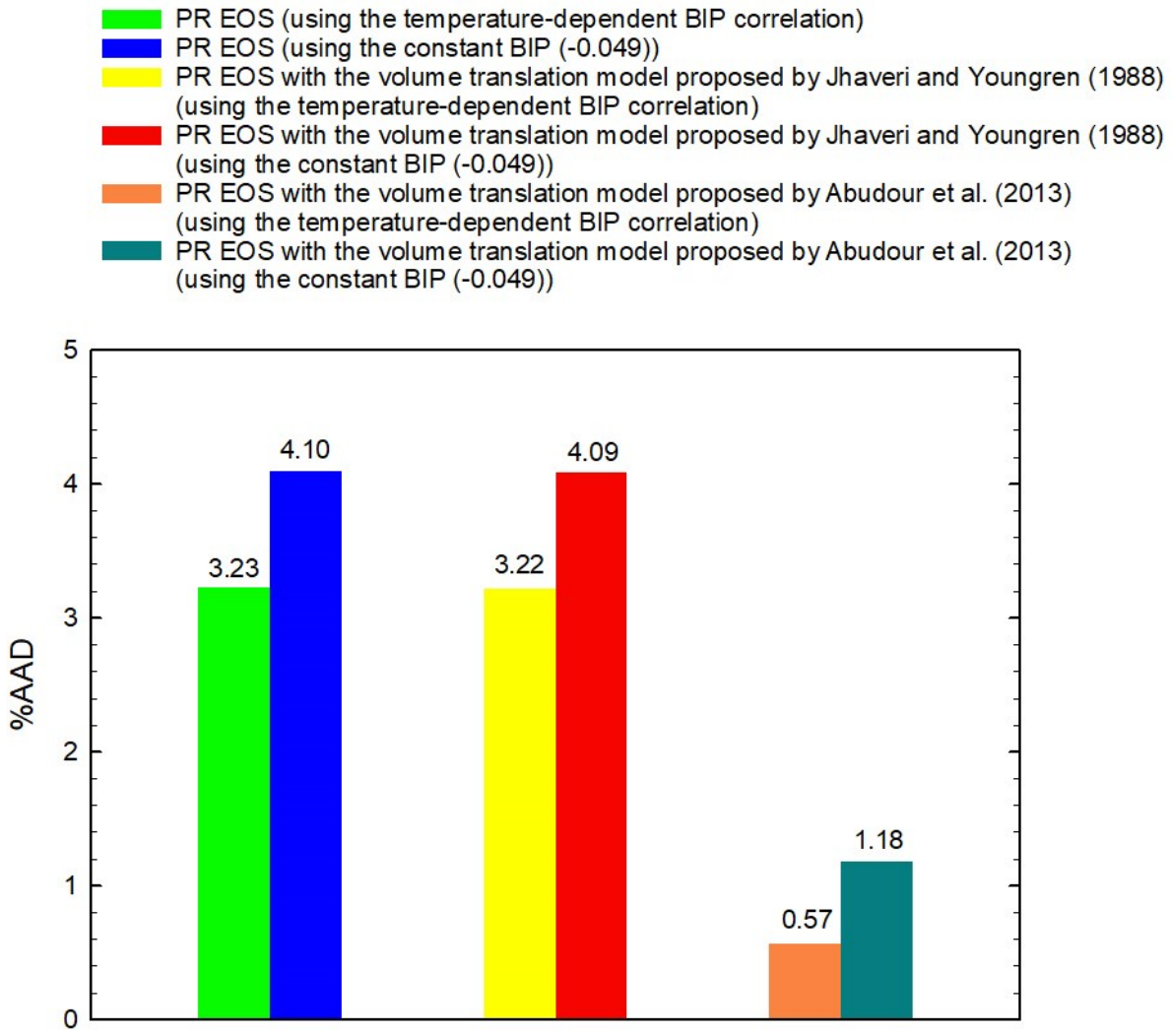


**Figure 3-4** Comparison between density calculation results using different density prediction models and BIPs.

### 3.2 Effect of DME Addition on MMP

In this section, MMP calculations are conducted on two oil samples with different compositions to show the effect of DME addition on MMP between $CO_2$ and crude oil. The MMC method proposed by Ahmadi and Johns (2011) is adopted for reliable MMP determinations. The effect of adding different amounts of DME on MMP is studied in each case study.

### 3.2.1 Case Study 1

Table 3-6 shows the composition of oil sample 1, which contains methane ($C_1$), butane ($C_4$), n-eicosane ($C_{20}$), and the composition of injection gases at 344.261 K. The compositions of Gas 2 and Gas 3 in Table 3-6 are designed to allow for the investigation on the effect of adding different amounts of DME on MMP. Table 3-7 shows the critical properties of each component in case study 1 used in the calculations. Table 3-8 shows the BIPs used in PR EOS. Note that the BIP value between $CO_2$ and DME is obtained from the temperature-dependent BIP correlation developed in this thesis. The other BIPs are obtained from the study by Ratnakar *et al*. (2017).

Figure 3-5 shows the minimum tie line lengths as a function of pressure for oil sample 1 displaced by Gas 1, Gas 2, and Gas 3 at 344.261 K. Figure 3-5 (a) presents the comparison of the minimum tie line lengths yielded by Gas 1, Gas 2, and Gas 3 containing 0, 10%, and 20% DME, respectively. The blue line is the minimum tie line length obtained for the displacement by Gas 1 (which contains 20% $C_1$ and 80% $CO_2$), while the green line is the minimum tie line length obtained for the displacement by Gas 2 (which contains 10% $C_1$, 80% $CO_2$, and 10% DME). The red line represents the minimum tie line length obtained for the displacement by Gas 3 (which contains 80% $CO_2$ and 20% DME). The resulting MMPs are predicted by the power-law extrapolation method. Figure 3-5 (b), Figure 3-5 (c) and Figure 3-5 (d) illustrate how to extrapolate the tie line lengths to zero values for the displacements by Gas 1, Gas 2, Gas 3, respectively. In Figure 3-5 (b), Figure 3-5 (c) and Figure 3-5 (d), the blue dots represent the calculated minimum tie line lengths at the last several pressures using the MMC method proposed by Ahmadi and Johns (2011); $R^2$ denotes the correlation coefficient, which is required to exceed 0.999 to achieve reliable MMP predictions (Ahmadi and Johns, 2011). In this case, all the $R^2$ values of the three displacements are larger than 0.999, ensuring the reliability of the predicted MMPs by the MMC method. As seen from Figure

3-5 (b), the predicted MMP is 161.88 bar, which matches well with the MMP (i.e., 158.79 bar) reported by Ahmadi and Johns (2011). The predicted MMPs in Figure 3-5 (c) and Figure 3-5(d) are 117.16 bar and 85.63 bar, respectively. Lastly, it can be observed from Figure 3-6 that adding DME is able to significantly reduce the MMP between this oil sample and $CO_2$-dominat gases.

Figure 3-7 presents the variation of the tie line lengths as a function of contact number for oil sample 1 displaced by Gas 1, Gas 2, and Gas 3 at 344.261 K when the minimum tie line length is approximately 0.2. Note that the contact number refers to the number of rows in Figure 2-1. As mentioned by Ahmadi and Johns (2011), the development of key tie line lengths versus contact number at the pressures slightly lower than MMP can illustrate the gas drive mechanisms. Five profiles of tie line lengths yielded at different contact times by the displacements of Gas 1, Gas 2, and Gas 3 are shown in Figure 3-7 (a), Figure 3-7 (b), and Figure 3-7 (c). As is shown in Figure 3-7, the key tie lines are nearly fully developed after the 25th contact. But, we consider the key tie lines at the 100th contact to be fully developed to ensure the accuracy in finding the minimum key tie line in this study. It can be seen from Figure 3-7 that the tie line in the middle of the contacts is the crossover tie line; the gas tie line is located on the left side of the crossover tie line, while the oil tie line lies on the right side of the crossover tie line. It can be seen from Figure 3-7 (a) that the crossover tie line is the shortest key tie line, indicating that a combined condensing and vaporizing drive controls the miscibility between oil sample 1 and Gas 1. In comparison, as seen in Figure 3-7 (b), the gas tie line is the shortest key tie line, indicating that the miscibility between oil sample 1 and Gas 2 is achieved by a condensing drive. Figure 3-7 (c) also shows the gas tie line is the shortest key tie line that controls the miscibility of oil sample 1 and Gas 3, demonstrating that a condensing drive controls miscibility between oil sample 1 and Gas 3. It can be seen from Figure 3-7 that DME addition into $CO_2$ makes the gas richer, which results in the alteration of the

miscibility mechanism from a combined condensing and vaporizing drive mechanism to a condensing drive mechanism.

**Table 3-6** Compositions of oil and three injection gases in mole percentages considered in case study 1 (Wang and Orr, 1997).

| Component | Oil sample 1 | Gas 1 | Gas 2[a] | Gas 3[a] |
|---|---|---|---|---|
| $C_1$ | 0.20 | 0.20 | 0.10 | 0 |
| $C_4$ | 0.15 | 0 | 0 | 0 |
| $C_{10}$ | 0.65 | 0 | 0 | 0 |
| $CO_2$ | 0 | 0.80 | 0.80 | 0.80 |
| DME | 0 | 0 | 0.10 | 0.20 |

[a] These are the compositions of injection gas generated by adding different amounts of DME.

**Table 3-7** Critical properties of components used in case study 1.

| Component | $T_c$ (bar) | $P_c$ (K) | $\omega$ |
|---|---|---|---|
| $C_1$[a] | 190.58 | 46.04 | 0.0104 |
| $C_4$[a] | 425.18 | 37.97 | 0.2010 |
| $C_{10}$[a] | 617.65 | 21.08 | 0.4900 |
| $CO_2$[b] | 304.20 | 73.83 | 0.2390 |
| DME[b] | 400.05 | 52.92 | 0.2000 |

[a] is retrieved from the paper by Orr *et al*. (1993).
[b] is retrieved from the paper by Tallon and Fenton (2010).

**Table 3-8** BIPs used in case study 1 (Ratnakar *et al*., 2017).

| Component | $C_1$ | $C_4$ | $C_{10}$ | $CO_2$ | DME |
|---|---|---|---|---|---|
| $C_1$ | 0 | 0 | 0 | 0.120 | 0.030 |
| $C_4$ | 0 | 0 | 0 | 0.120 | 0.050 |
| $C_{10}$ | 0 | 0 | 0 | 0.100 | 0.015 |
| $CO_2$ | 0.120 | 0.120 | 0.100 | 0 | -0.013[a] |
| DME | 0.030 | 0.050 | 0.015 | -0.013[a] | 0 |

[a] These data are obtained from the regressed BIP correlation for $CO_2$-DME binary.

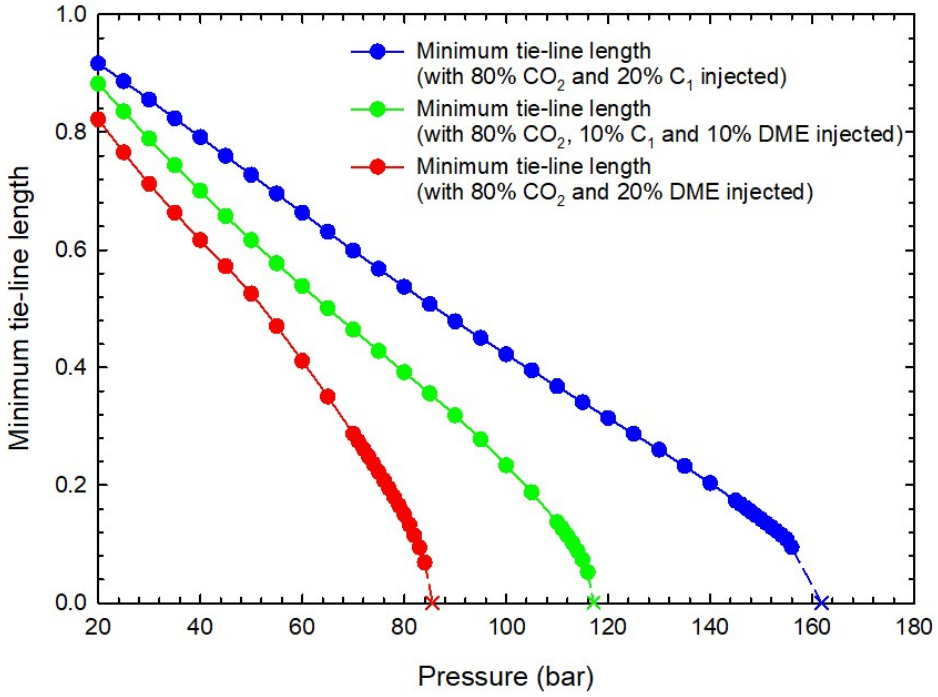
Minimum tie-line length
(with 80% CO2 and 20% C1 injected)
Minimum tie-line length
(with 80% CO2, 10% C1 and 10% DME injected)
Minimum tie-line length
(with 80% CO2 and 20% DME injected)
Minimum tie-line length
Pressure (bar)
1.0
0.8
0.6
0.4
0.2
0.0
20
40
60
80
100
120
140
160
180

(a)

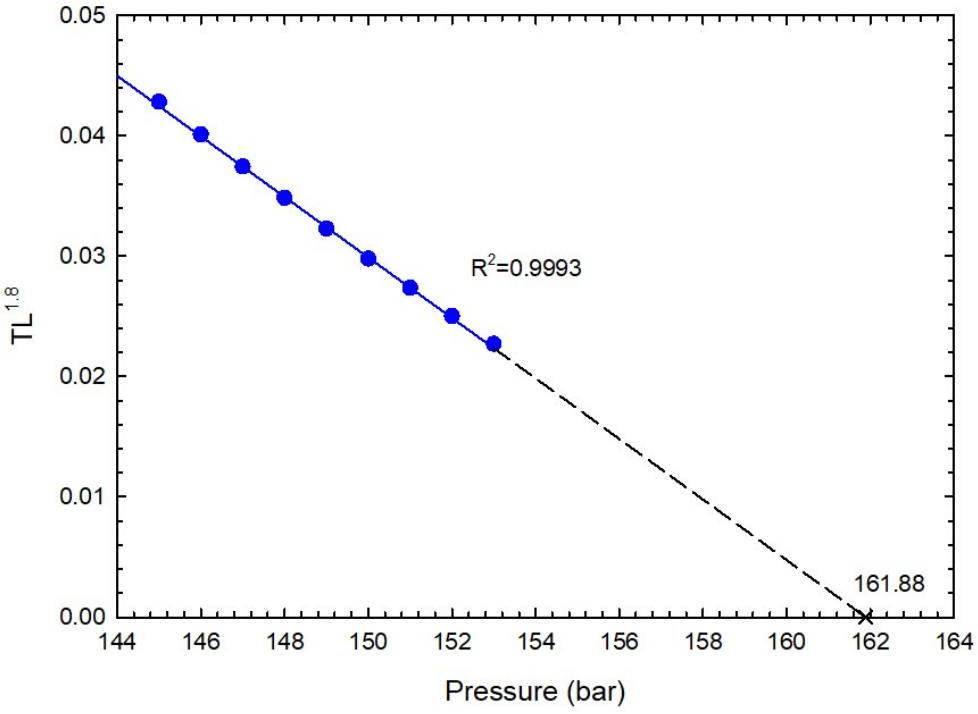
R2=0.9993
161.88
TL1.8
Pressure (bar)
0.05
0.04
0.03
0.02
0.01
0.00
144
146
148
150
152
154
156
158
160
162
164

(b)

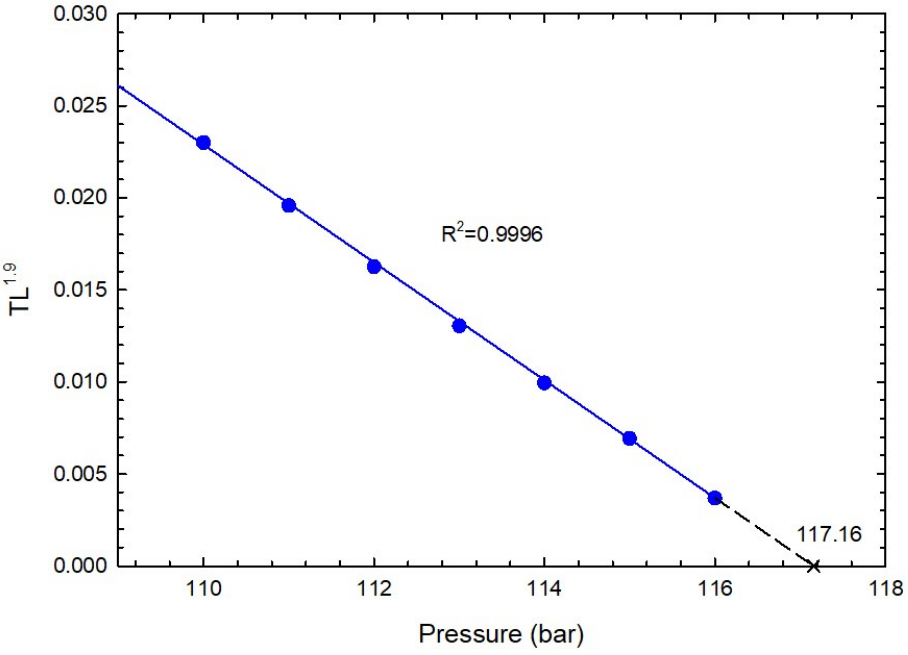


(c)

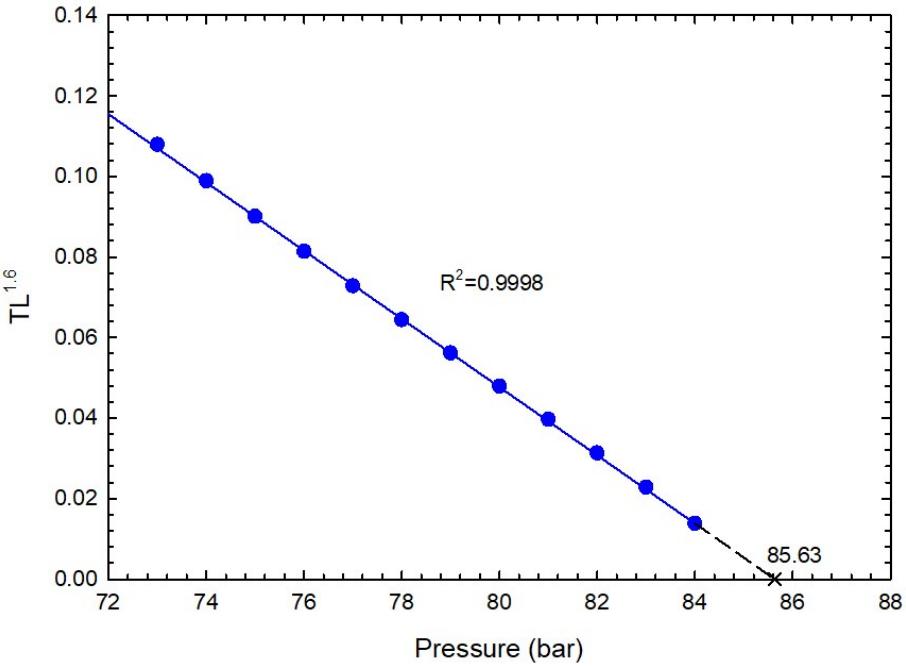


(d)

**Figure 3-5** The minimum tie line lengths as a function of pressure for the oil in case study 1 displaced by Gas 1, Gas 2, and Gas 3 at 344.261 K. (a) Comparison of the minimum tie line lengths yielded by Gas 1, Gas 2, and Gas 3, which contain 0, 10%, and 20% DME, respectively; (b) Extrapolation of the tie line lengths to zero for the displacement by Gas 1; (c) Extrapolation of the tie line lengths to zero for the displacement by Gas 2; (d) Extrapolation of the tie line lengths to zero for the displacement by Gas 3.

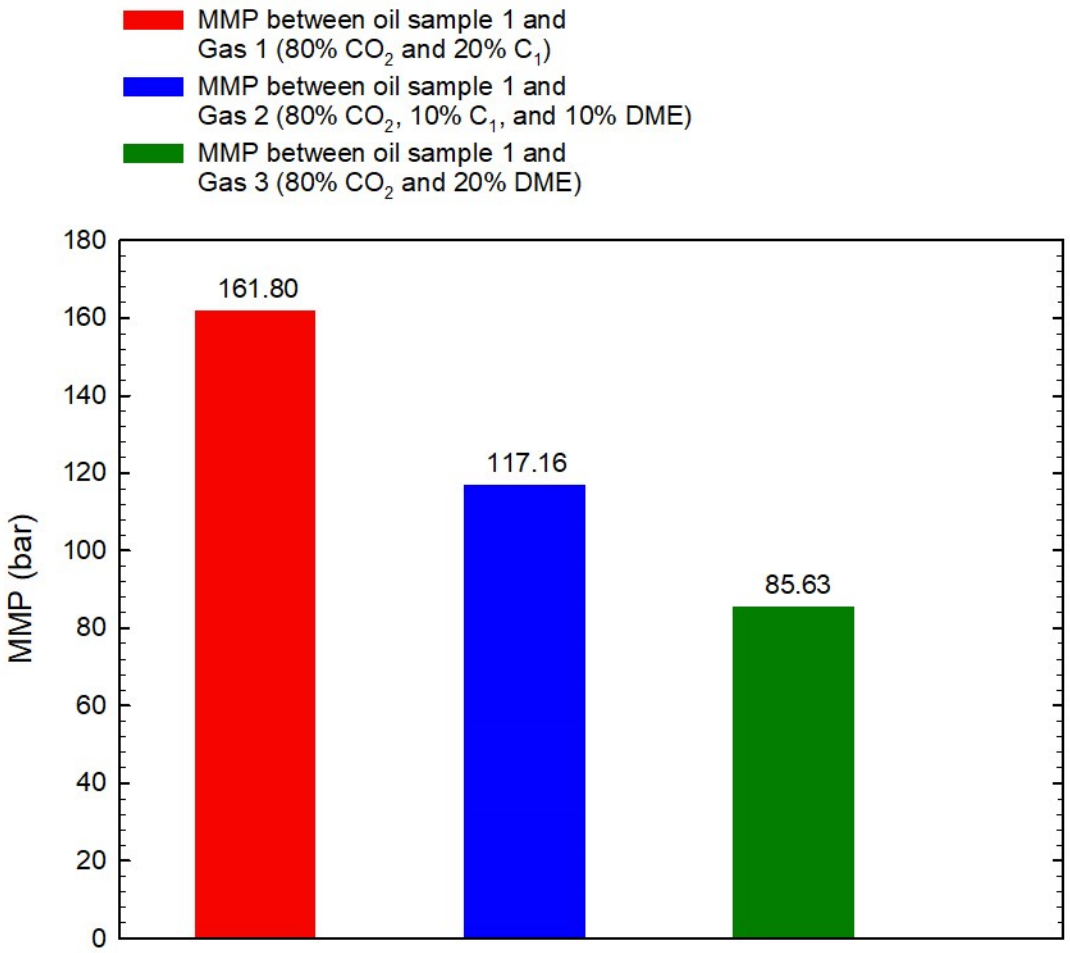


**Figure 3-6** Comparison of the MMPs yielded by Gas 1, Gas 2, and Gas 3, which contain 0, 10%, and 20% DME, respectively.

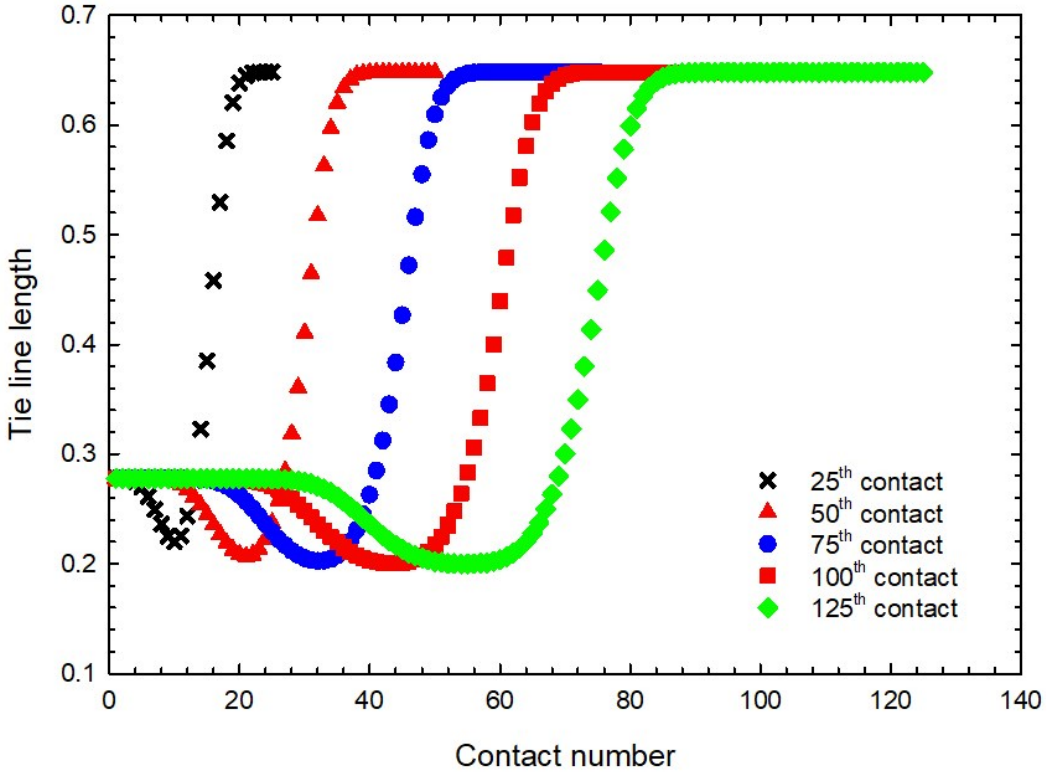
Tie line length
Contact number
25th contact
50th contact
75th contact
100th contact
125th contact

(a)

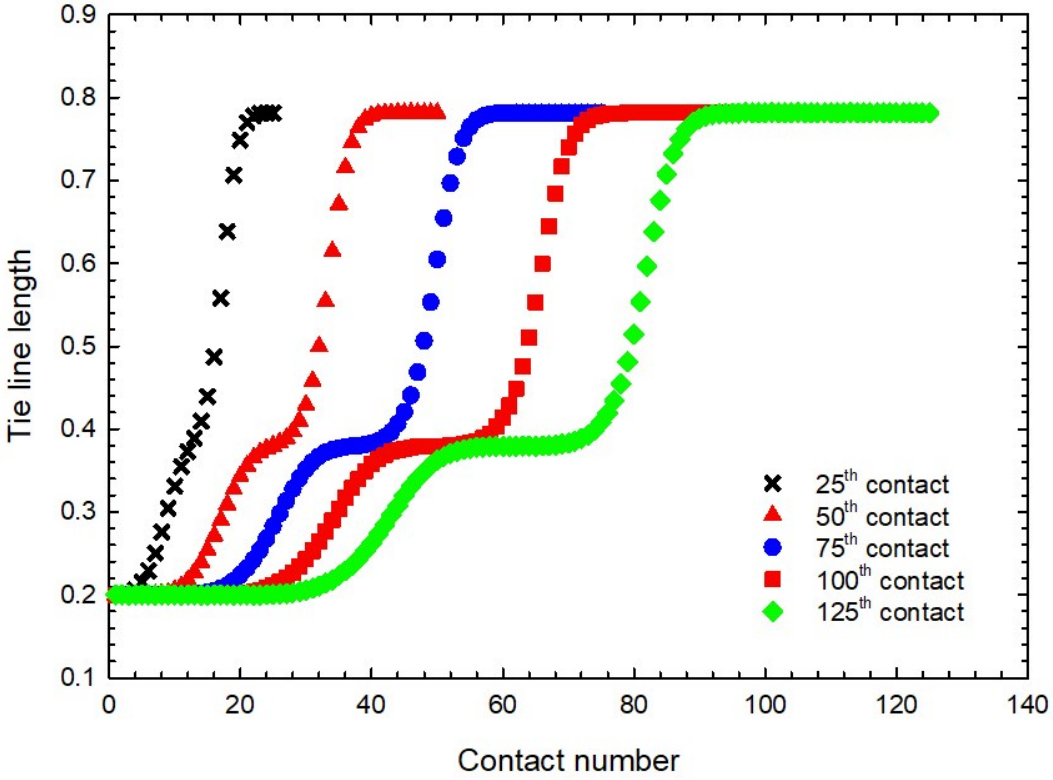
Tie line length
Contact number
25th contact
50th contact
75th contact
100th contact
125th contact

(b)

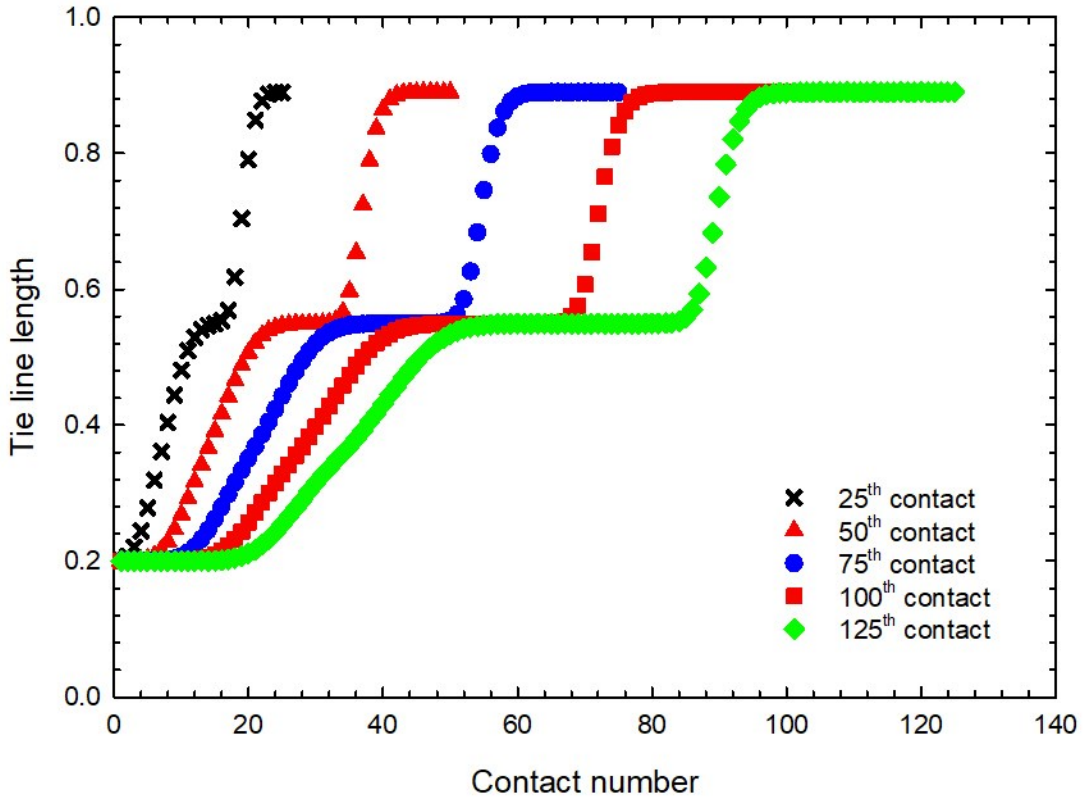


(c)

**Figure 3-7** Variation of the tie line lengths as a function of contact number at 344.261 K and different pressures when the oil sample 1 is displaced by (a) Gas 1; (b) Gas 2, which contains 10% DME; (c) Gas 3, which contains 20% DME. For each case, the minimum tie line length is around 0.2.

### 3.2.2 Case Study 2

The compositions of oil sample 2 and three injection gases are listed in Table 3-9. Table 3-10 presents the critical properties of components used in case study 2. Table 3-11 shows the BIPs used in this case study. Note that the BIP between $CO_2$ and DME is calculated by the temperature-dependent BIP correlation developed in this thesis. Figure 3-8 depicts the minimum tie line lengths as a function of pressure which are obtained when the oil sample 2 is displaced by Gas 4, Gas 5,

and Gas 6 at 322.039 K. Figure 3-8 (a) shows the relationship between minimum tie line lengths and pressure when the oil sample 2 is displaced by Gas 4, Gas 5, and Gas 6, respectively. The blue line, the green line, and the red line represent the results of displacement by Gas 4, Gas 5, and Gas6, respectively. Then the MMPs are determined using the power-law extrapolation method. Figure 3-8 (b), Figure 3-8 (c), and Figure 3-8 (d) present the extrapolation of the minimum tie line lengths to zero values yielded by the displacements by Gas 4, Gas 5, and Gas 6. Again, Figure 3-8 shows that the $R^2$ values obtained in the three displacements are all larger than 0.999, which ensures the reliability of the predicted MMPs by the MMC method. The MMP of oil displaced by Gas 4 is 91.23 bar, which is consistent with the MMP value of 88.46 bar reported by Ahmadi and Johns (2011). It can be seen from Figure 3-8 (c) and Figure 3-8 (d) that the MMPs obtained with the use of Gas 5 and Gas 6 are predicted to 87.07 bar and 81.46 bar, respectively. Lastly, the bar charts drawn in Figure 3-9 clearly demonstrates that adding DME into $CO_2$ can reduce the MMP between injection gas and reservoir oil. The value of MMPs can be further reduced with an increasing amount of added DME. But it is noted that the degree of MMP reduction obtained for this oil sample is much lower than that obtained for oil sample 1. Therefore, the degree of MMP reduction caused by DME addition seems to vary with the composition/properties of oil samples.

Figure 3-10 presents the variation of the tie line lengths as a function of contact number for oil sample 2 displaced by Gas 4, Gas 5, and Gas 6 at 322.039 K and 70 bar. Note that 70 bar is selected because this pressure level is close to MMP and the minimum tie line lengths at this pressure for the displacements by Gas 4, Gas 5, and Gas 6 are relatively low. Five profiles of tie line lengths yielded at different contact times by the displacements of Gas 4, Gas 5, and Gas 6 are shown in Figure 3-10 (a), Figure 3-10 (b), and Figure 3-10 (c). As is shown in Figure 3-10, the key tie lines are gradually developed with an increase of contact numbers. It can be seen from Figure 3-10 (a)

that one of the crossover tie lines is the shortest key tie line, indicating that a combined condensing and vaporizing drive controls the miscibility between oil sample 2 and Gas 4 (i.e., pure $CO_2$). As seen in Figure 3-10 (b), the one of the crossover tie lines is the shortest key tie line, demonstrating that the miscibility between oil sample 2 and Gas 5 is achieved by a combined condensing and vaporizing drive. Figure 3-10 (c) also shows one of the crossover tie lines is the shortest key tie line, indicating that the miscibility between oil sample 2 and Gas 6 is achieved via a combined condensing and vaporizing drive.

**Table 3-9** Compositions of the crude oil and three injection gases in mole percentages considered in case study 2 (Johns and Orr, 1996).

| Component | Oil sample 2 | Gas 4 | Gas 5[a] | Gas 6[a] |
|---|---|---|---|---|
| DME | 0 | 0 | 0.05 | 0.10 |
| $CO_2$ | 0 | 1 | 0.95 | 0.90 |
| Methane ($C_1$) | 0.35 | 0 | 0 | 0 |
| Ethane ($C_2$) | 0.03 | 0 | 0 | 0 |
| Propane ($C_3$) | 0.04 | 0 | 0 | 0 |
| Butane ($C_4$) | 0.06 | 0 | 0 | 0 |
| Pentane ($C_5$) | 0.04 | 0 | 0 | 0 |
| Hexane ($C_6$) | 0.03 | 0 | 0 | 0 |
| Heptane ($C_7$) | 0.05 | 0 | 0 | 0 |
| Octane ($C_8$) | 0.05 | 0 | 0 | 0 |
| Decane ($C_{10}$) | 0.30 | 0 | 0 | 0 |
| n-tetradecane ($C_{14}$) | 0.05 | 0 | 0 | 0 |

[a] These are the compositions of injection gas generated by adding different amounts of DME.

**Table 3-10** Critical properties of components used in case study 2.

| Component | $T_c$ (bar) | $P_c$ (K) | $\omega$ |
|---|---|---|---|
| DME[a] | 400.05 | 52.92 | 0.2000 |
| $CO_2$[a] | 304.22 | 73.83 | 0.2310 |
| $C_1$[b] | 190.56 | 46.04 | 0.0115 |
| $C_2$[b] | 305.44 | 48.80 | 0.0908 |
| $C_3$[b] | 369.83 | 42.49 | 0.1454 |
| $C_4$[b] | 425.17 | 37.97 | 0.1928 |
| $C_5$[b] | 469.67 | 33.69 | 0.2510 |
| $C_6$[b] | 507.78 | 32.82 | 0.2710 |
| $C_7$[b] | 542.22 | 31.51 | 0.3100 |
| $C_8$[b] | 570.56 | 29.51 | 0.3490 |
| $C_{10}$[b] | 622.22 | 25.30 | 0.4370 |
| $C_{14}$[b] | 700.55 | 19.58 | 0.6010 |

[a] These data are retrieved from Tallon and Fenton (2010).

[b] These data are retrieved from Johns and Orr (1996).

**Table 3-11** BIPs used in case study 2 (Ratnakar *et al*., 2017).

| Component | DME | $CO_2$ | $C_1$ | $C_2$ | $C_3$ | $C_4$ | $C_5$ | $C_6$ | $C_7$ | $C_8$ | $C_{10}$ | $C_{14}$ |
|---|---|---|---|---|---|---|---|---|---|---|---|---|
| DME | 0 | -0.018[a] | 0.030 | 0.050 | 0.050 | 0.050 | 0.020 | 0.020 | 0.022 | 0.020 | 0.015 | 0.006 |
| $CO_2$ | -0.018[a] | 0 | 0.120 | 0.120 | 0.120 | 0.120 | 0.120 | 0.120 | 0.100 | 0.100 | 0.100 | 0.100 |
| $C_1$ | 0.030 | 0.120 | 0 | 0 | 0 | 0 | 0 | 0 | 0 | 0 | 0 | 0 |
| $C_2$ | 0.050 | 0.120 | 0 | 0 | 0 | 0 | 0 | 0 | 0 | 0 | 0 | 0 |
| $C_3$ | 0.050 | 0.120 | 0 | 0 | 0 | 0 | 0 | 0 | 0 | 0 | 0 | 0 |
| $C_4$ | 0.050 | 0.120 | 0 | 0 | 0 | 0 | 0 | 0 | 0 | 0 | 0 | 0 |
| $C_5$ | 0.020 | 0.120 | 0 | 0 | 0 | 0 | 0 | 0 | 0 | 0 | 0 | 0 |
| $C_6$ | 0.020 | 0.120 | 0 | 0 | 0 | 0 | 0 | 0 | 0 | 0 | 0 | 0 |
| $C_7$ | 0.022 | 0.100 | 0 | 0 | 0 | 0 | 0 | 0 | 0 | 0 | 0 | 0 |
| $C_8$ | 0.020 | 0.100 | 0 | 0 | 0 | 0 | 0 | 0 | 0 | 0 | 0 | 0 |
| $C_{10}$ | 0.015 | 0.100 | 0 | 0 | 0 | 0 | 0 | 0 | 0 | 0 | 0 | 0 |
| $C_{14}$ | 0.006 | 0.100 | 0 | 0 | 0 | 0 | 0 | 0 | 0 | 0 | 0 | 0 |

[a] These data are obtained from the temperature-dependent BIP correlation for $CO_2$-DME mixture developed in this thesis.

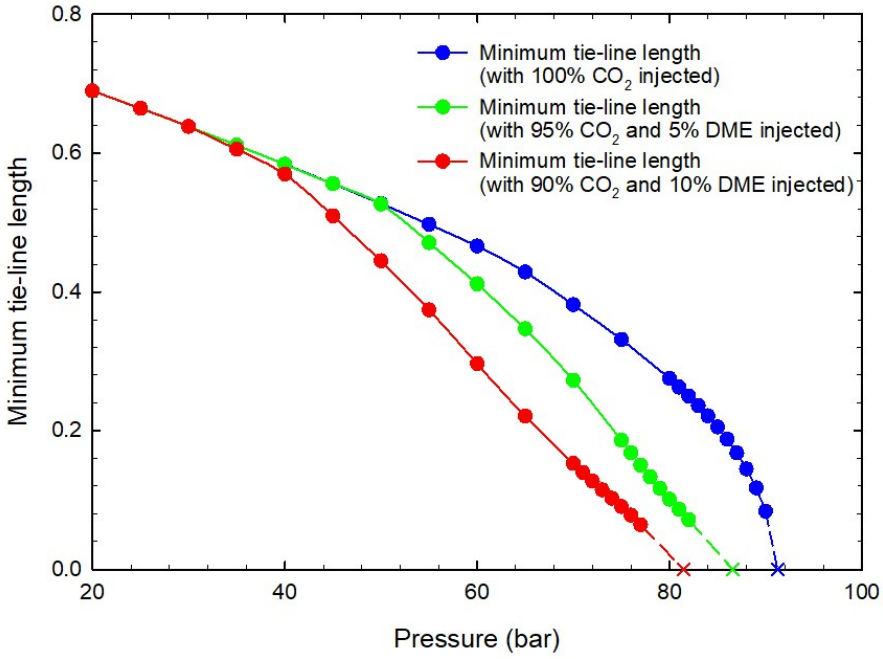
Minimum tie-line length
(with 100% $CO_2$ injected)
Minimum tie-line length
(with 95% $CO_2$ and 5% DME injected)
Minimum tie-line length
(with 90% $CO_2$ and 10% DME injected)
Minimum tie-line length
Pressure (bar)
0.0
0.2
0.4
0.6
0.8
20
40
60
80
100

(a)

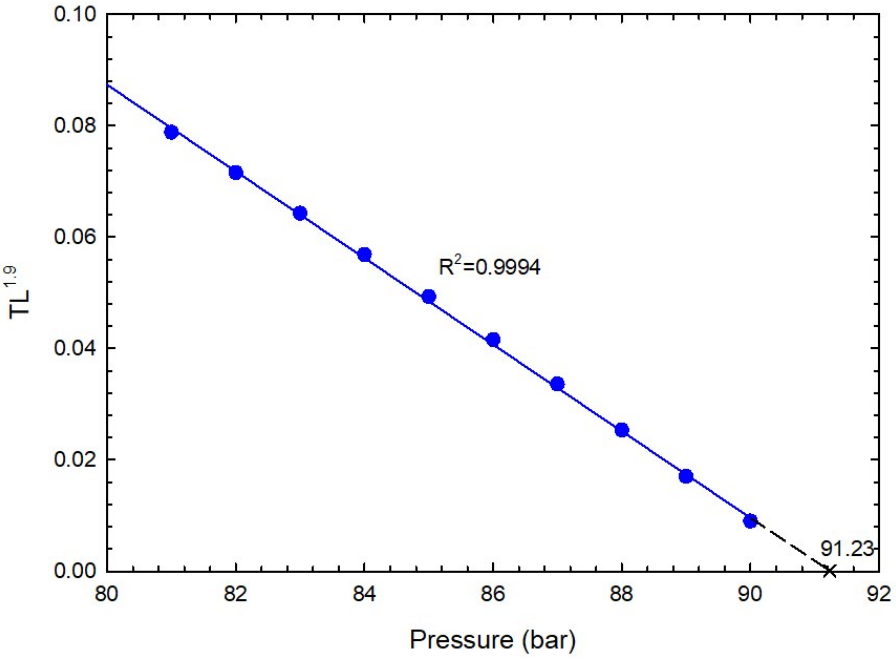
$R^2$=0.9994
91.23
$TL^{1.9}$
Pressure (bar)
0.00
0.02
0.04
0.06
0.08
0.10
80
82
84
86
88
90
92

(b)

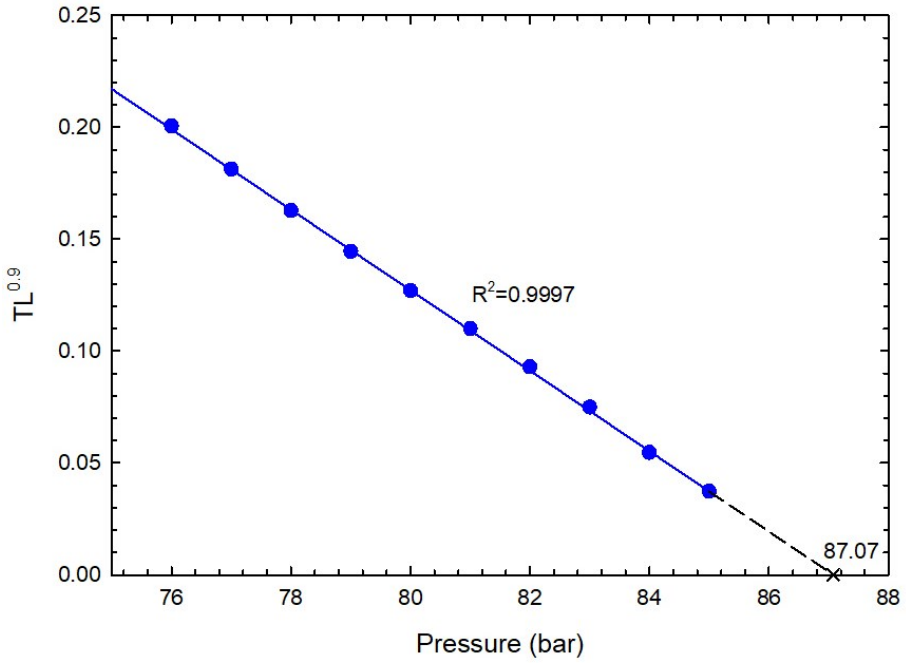


(c)

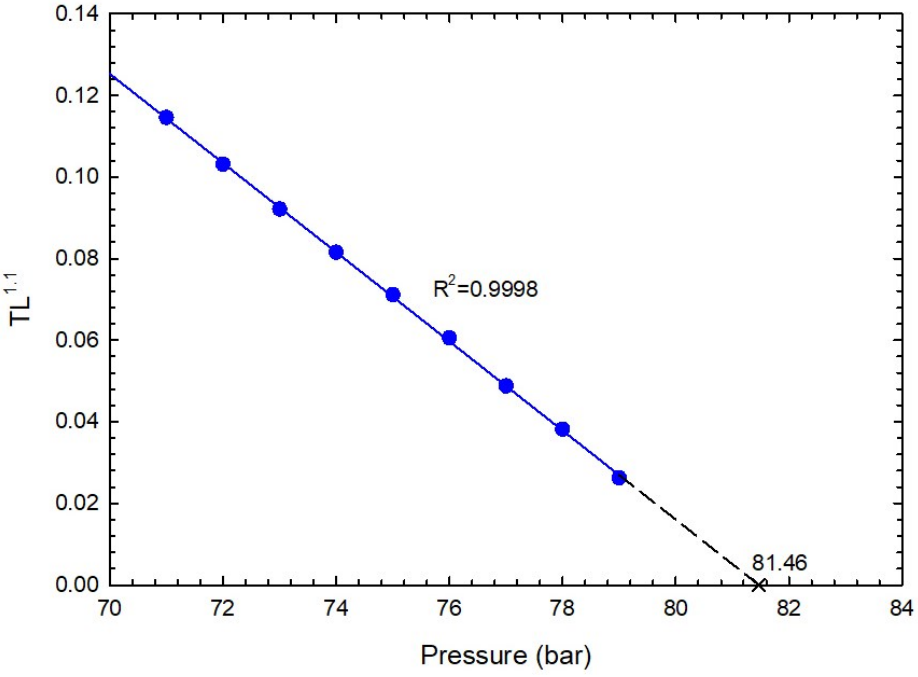


(d)

**Figure 3-8** The minimum tie line lengths as a function of pressure obtained for the oil sample 2 displaced by Gas 4, Gas 5, and Gas 6 at 322.039 K. (a) Comparison of the minimum tie line lengths yielded by Gas 4, Gas 5, and Gas 6, which contain 0, 5%, and 10% DME, respectively; (b) Extrapolation of the tie line lengths to zero for the displacement by Gas 4; (c) Extrapolation of the tie line lengths to zero for the displacement by Gas 5; (d) Extrapolation of the tie line lengths to zero for the displacement by Gas 6.

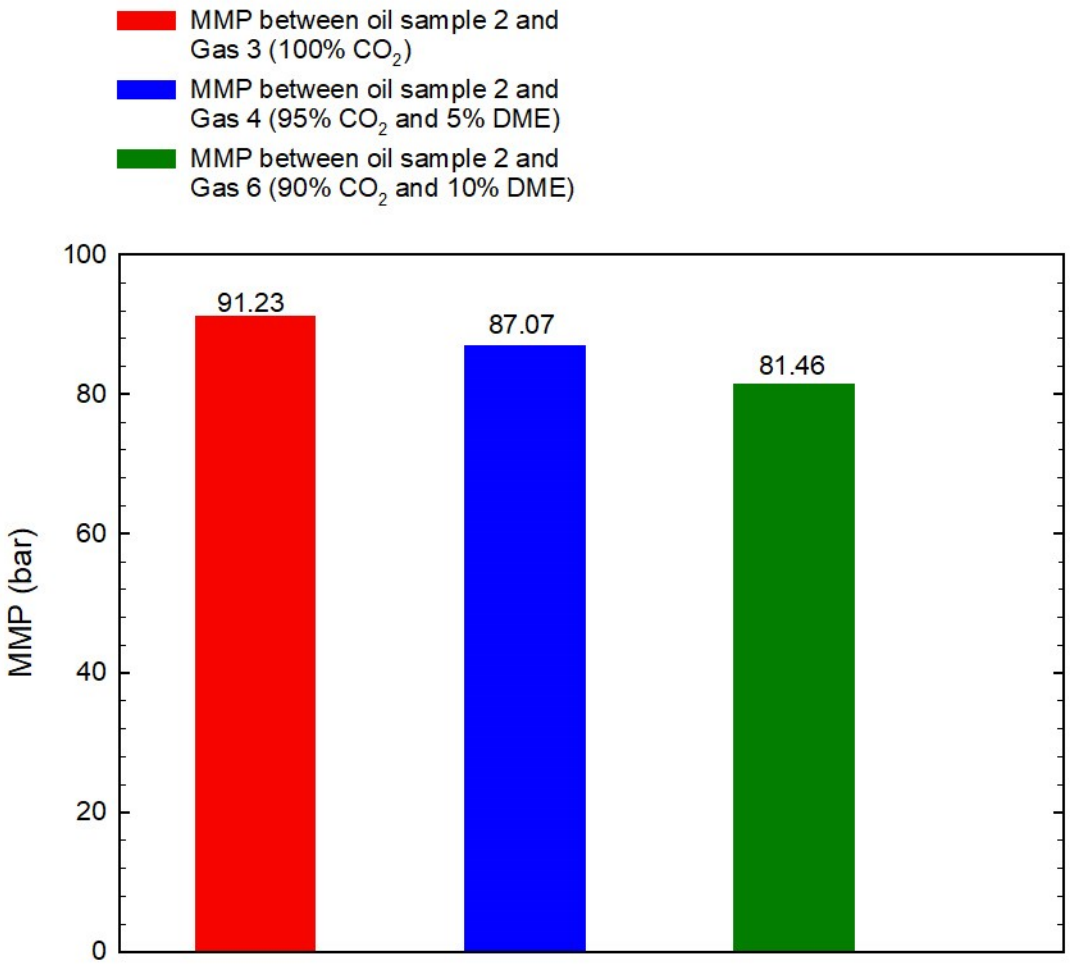


**Figure 3-9** Comparison of MMPs yielded by Gas 4, Gas 5, and Gas 6, which contain 0, 5%, and 10% DME, respectively.

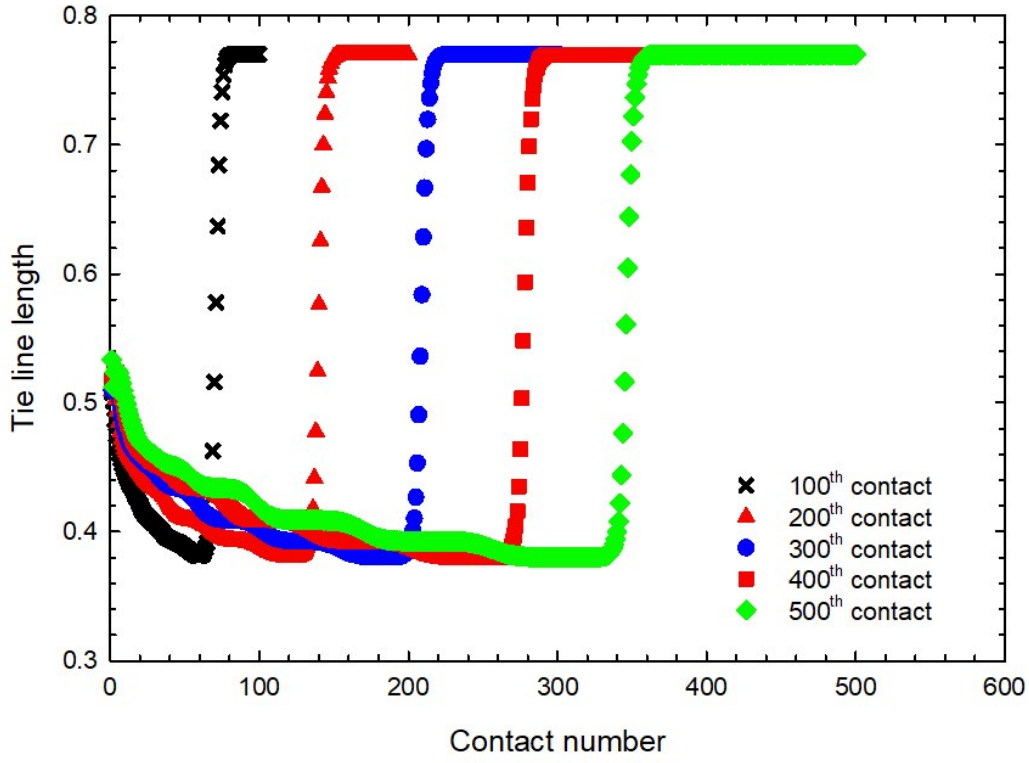
Tie line length
Contact number
100th contact
200th contact
300th contact
400th contact
500th contact

(a)

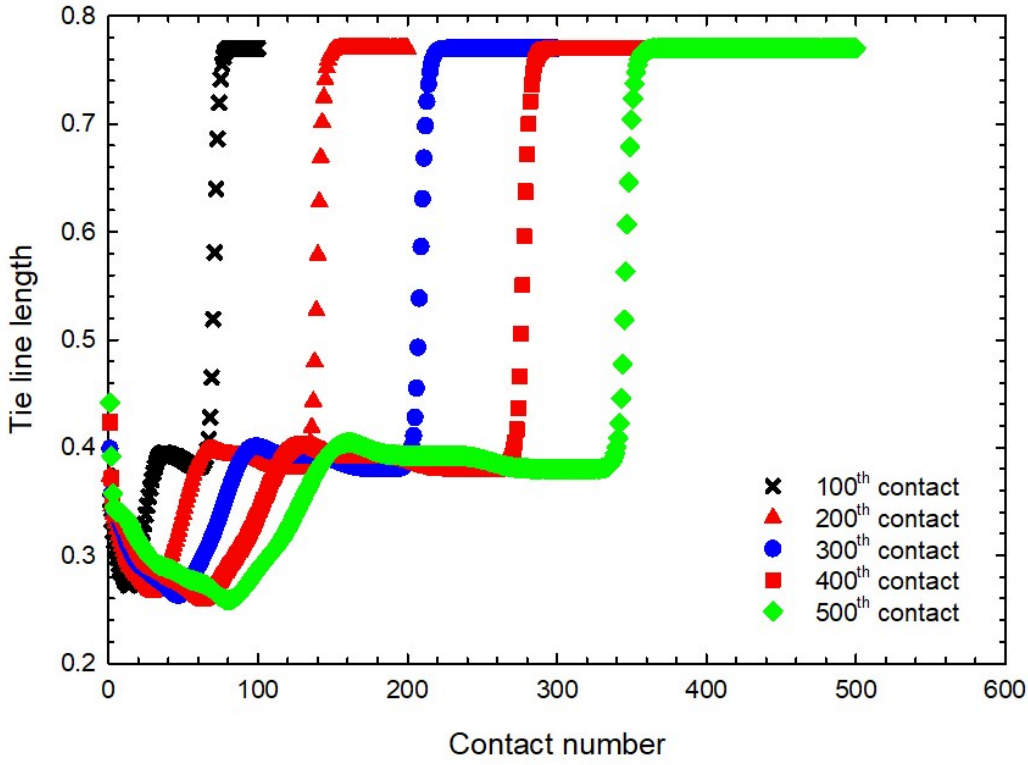
Tie line length
Contact number
100th contact
200th contact
300th contact
400th contact
500th contact

(b)

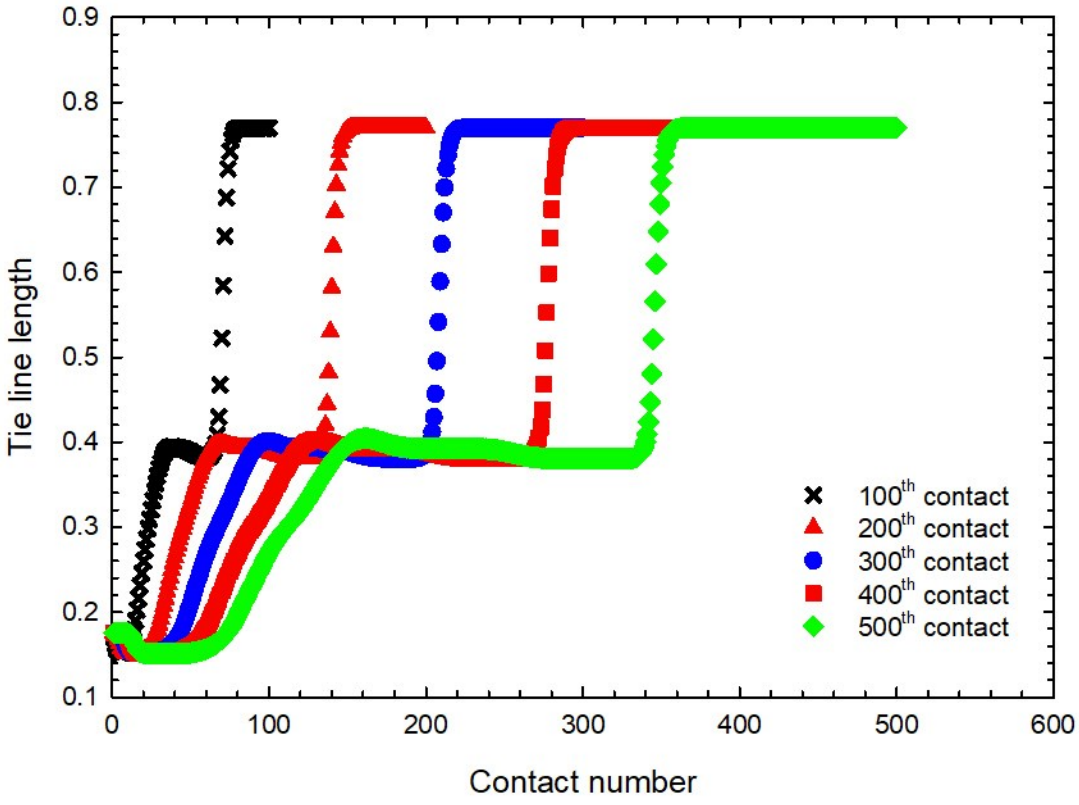


(c)

**Figure 3-10** Variation of the tie line lengths at 322.039 K and 70 bar as a function of contact number for oil sample 2 displaced by (a) Gas 4; (b) Gas 5, which contains 5% DME; (c) Gas 6, which contains 10% DME.

**References**

Abudour, A.M., Mohammad, S.A., Gasem, K.A., 2012b. Modeling high-pressure phase equilibria of coalbed gases/water mixtures with the Peng-Robinson equation of state. Fluid Phase Equilibr. 319, 77-89.

Abudour, A.M., Mohammad, S.A., Robinson Jr, R.L., Gasem, K.A., 2013. Volume-translated Peng-Robinson equation of state for liquid densities of diverse binary mixtures. Fluid Phase Equilibr. 349, 37-55.

Ahmadi, K., Johns, R.T., 2011. Multiple-mixing-cell method for MMP calculations. SPE J. 16 (04), 733-742.

Jhaveri, B.S., Youngren, G.K., 1988. Three-parameter modification of the Peng-Robinson equation of state to improve volumetric predictions. SPE Res. Eng. 3 (03), 1-033.

Johns, R.T., Orr, F.M., 1996. Miscible gas displacement of multicomponent oils. SPE J. 1 (01), 39-50.

Orr, F.M., Johns, R.T., Dindoruk, B., 1993. Development of miscibility in four-component $CO_2$ floods. SPE Res. Eng. 8 (02), 135-142.

Ratnakar, R.R., Dindoruk, B., Wilson, L.C., 2017. Phase behavior experiments and PVT modeling of DME-brine-crude oil mixtures based on Huron-Vidal mixing rules for EOR applications. Fluid Phase Equilibr. 434, 49-62.

Rowley, R.L., Wilding, W.V., Oscarson, J.L., 2007. DIPPR Project 801 data compilation of pure compound properties, AIChE DIPPR. New York.

Tallon, S., Fenton, K., 2010. The solubility of water in mixtures of dimethyl ether and carbon dioxide. Fluid Phase Equilibr. 298 (1), 60-66.

Tsang, C.Y., Streett, W.B., 1981. Vapor-liquid equilibrium in the system carbon dioxide/dimethyl ether. J. Chem. Eng. Data. 26 (2), 155-159.

Wang, Y., Orr, F.M., 1997. Analytical calculation of minimum miscibility pressure. Fluid Phase Equilibr. 139 (1-2), 101-124.

# CHAPTER 4 CONCLUSIONS AND RECOMMENDATIONS

Phase behaviour of $CO_2$-DME binary plays an important role in affecting the efficiency of recovery processes that uses $CO_2$ and DME as injection agents. In this thesis, the experimental VLE data of $CO_2$-DME system at different temperatures and pressures are first collected from the literature. These VLE data are then used to regress a linear temperature-dependent BIP correlation in PR EOS. To achieve accurate density predictions, PR EOS is coupled with three volume translation models in the density prediction for $CO_2$-DME binary. Calculation results are then compared with the experimental data (Tallon and Fenton, 2010) to test the accuracy of each volume translation model. To investigate the effect of DME addition on the MMP between $CO_2$ and crude oil, the MMC method proposed by Ahmadi and Johns (2011) is used to carry out MMP calculations between two oil samples and different injection gases with varied amounts of DME. Conclusions from this thesis and recommendations for future study are provided in this chapter.

## 4.1. Conclusions

From the calculation results, we can conclude that significant improvements in reproducing the VLE composition data for $CO_2$-DME binary have been achieved by adopting the temperature-dependent BIPs as compared to the case with the use of a constant BIP. The accuracy of density predictions for $CO_2$-DME mixtures is also improved by using the temperature-dependent BIP correlation. Compared to the constant volume translation model by Jhaveri and Youngren (1988), the volume translation model that is proposed by Abudour *et al*. (2013) together with the newly developed BIP correlation provides more accurate density predictions for $CO_2$-DME mixtures, yielding a low error of only 0.57%AAD. The MMP calculation results show that adding DME in injection gas can lower the MMP, and a higher DME dosage leads to a lower MMP. But the degree of MMP reduction caused by DME addition seems to depend on the composition/properties of the

oil samples. In addition, the gas drive mechanism may be altered by DME addition. DME addition into $CO_2$ makes the injection gas richer, which results in the alteration of the miscibility mechanism from a combined condensing and vaporizing drive mechanism to a condensing drive mechanism.

### 4.2. Recommendations

- In this work, we only consider the phase equilibrium between $CO_2$, DME, and oil. However, water also frequently appears in reservoirs. Therefore, a three-phase vapor-liquid-aqueous flash algorithm might be necessary to better model the phase behavior of $CO_2$-DME-oil mixtures;
- The three-phase vapor-liquid-aqueous flash algorithm can be coupled with the MMC code to investigate the presence of DME and water on the MMP and recovery efficiency of $CO_2$ flooding process;
- More thorough experimental and theoretical study on the phase behavior of DME-hydrocarbon mixtures should be carried out to optimize the BIPs between DME and various hydrocarbons;
- Slim-tube experiments should be conducted in the future to validate the calculated MMPs for the $CO_2$-DME-oil mixtures examined in this study.

**References**

Abudour, A.M., Mohammad, S.A., Robinson Jr, R.L., Gasem, K.A., 2013. Volume-translated Peng-Robinson equation of state for liquid densities of diverse binary mixtures. Fluid Phase Equilibr. 349, 37-55.

Ahmadi, K., Johns, R.T., 2011. Multiple-mixing-cell method for MMP calculations. SPE J. 16 (04), 733-742.

Jhaveri, B.S., Youngren, G.K., 1988. Three-parameter modification of the Peng-Robinson equation of state to improve volumetric predictions. SPE Res. Eng. 3 (03), 1-033.

Tallon, S., Fenton, K., 2010. The solubility of water in mixtures of dimethyl ether and carbon dioxide. Fluid Phase Equilibr. 298 (1), 60-66.

# BIBLIOGRAPHY

Aalto, M., Keskinen, K.I., Aittamaa, J., Liukkonen, S., 1996. An improved correlation for compressed liquid densities of hydrocarbons. Part 2. Mixtures. Fluid Phase Equilibr. 114 (1-2), 21-35.

Abudour, A.M., Mohammad, S.A., Gasem, K.A., 2012b. Modeling high-pressure phase equilibria of coalbed gases/water mixtures with the Peng–Robinson equation of state. Fluid Phase Equilibr. 319, 77-89.

Abudour, A.M., Mohammad, S.A., Robinson Jr, R.L., Gasem, K.A., 2012a. Volume-translated Peng-Robinson equation of state for saturated and single-phase liquid densities. Fluid Phase Equilibr. 335, 74-87.

Abudour, A.M., Mohammad, S.A., Robinson Jr, R.L., Gasem, K.A., 2013. Volume-translated Peng-Robinson equation of state for liquid densities of diverse binary mixtures. Fluid Phase Equilibr. 349, 37-55.

Ahlers, J., Gmehling, J., 2001. Development of an universal group contribution equation of state: I. Prediction of liquid densities for pure compounds with a volume translated Peng-Robinson equation of state. Fluid Phase Equilibr. 191 (1-2), 177-188.

Ahmadi, K., Johns, R.T., 2011. Multiple-mixing-cell method for MMP calculations. SPE J. 16 (04), 733-742.

Baled, H., Enick, R.M., Wu, Y., McHugh, M.A., Burgess, W., Tapriyal, D., Morreale, B.D., 2012. Prediction of hydrocarbon densities at extreme conditions using volume-translated SRK and

PR equations of state fit to high temperature, high pressure PVT data. Fluid Phase Equilibr. 317, 65-76.

Bell, I.H., Welliquet, J., Mondejar, M.E., Bazyleva, A., Quoilin, S., Haglind, F., 2019. Application of the group contribution volume translated Peng-Robinson equation of state to new commercial refrigerant mixtures. Int. J. Refrig. 103, 316-328.

Blom, C.P.A., Hedden, R., Matzakos, A.N., Uehara-Nagamine, E., 2013. Oil recovery process, USA Patent US20130161010A1.

Catchpole, O.J., Tallon, S.J., Eltringham, W.E., Grey, J.B., Fenton, K.A., Vagi, E.M., Vyssotski, M.V., MacKenzie, A.N., Ryan, J., Zhu, Y., 2009. The extraction and fractionation of specialty lipids using near critical fluids. J. Supercrit. Fluid. 47 (3), 591-597.

Cho, J., Kim, T.H., Lee, K.S., 2018. Compositional modeling and simulation of dimethyl ether (DME)- enhanced waterflood to investigate oil mobility improvement. Pet. Sci. 15, 297-304.

Chou, G.F., Prausnitz, J.M., 1989. A phenomenological correction to an equation of state for the critical region. AIChE J. 35 (9), 1487-1496.

Chueh, P.L., Prausnitz, J.M., 1967. Vapor-liquid equilibria at high pressures: calculation of critical temperatures, volumes, and pressures of nonpolar mixtures. AIChE J. 13 (6), 1107-1113.

Enick, R.M., Olsen, D.K., Ammer, J.R., Schuller, W., 2012. Mobility and conformance control for $CO_2$ EOR via thickeners, foams, and gels-a literature review of 40 Years of research and pilot tests. SPE 154122.

Flowers, P., Neth, E.J., Theopold, K., Langley, R., Robinson, W.R., 2018. Chemistry: Atoms First. OpenStax and the University of Connecticut and UConn Undergraduate Student Government Association.

Frey, K., Modell, M., Tester, J.W., 2009. Density-and-temperature-dependent volume translation for the SRK EOS: 1. Pure fluids. Fluid Phase Equilibr. 279 (1), 56-63.

Frey, K., Modell, M., Tester, J.W., 2013. Density-and-temperature-dependent volume translation for the SRK EOS: 2. Mixtures. Fluid Phase Equilibr. 343, 13-23.

Fried, J.J., Combarnous, M.A., 1971. Dispersion in porous media (Vol. 7). Elsevier.

Haszeldine, R.S., 2009. Carbon capture and storage: how green can black be? Sci. 325 (5948), 1647-1652.

Jaramillo, P., Griffin, W.M., McCoy, S.T., 2009. Life cycle inventory of $CO_2$ in an enhanced oil recovery system. Environ. Sci. Technol. 43, 8027-8032.

Jarrell, P.M., Fox, C.E., Stein, M.H., Webb, S.L., 2002. Practical aspects of $CO_2$ flooding (Vol. 22). Richardson, TX: Society of Petroleum Engineers.

Jaubert, J.N., Arras, L., Neau, E., Avaullee, L., 1998b. Properly defining the classical vaporizing and condensing mechanisms when a gas is injected into a crude oil. Ind. Eng. Chem. Res. 37 (12), 4860-4869.

Jaubert, J.N., Privat, R., Le Guennec, Y., Coniglio, L., 2016. Note on the properties altered by application of a Péneloux-type volume translation to an equation of state. Fluid Phase Equilibr. 419, 88-95.

Jaubert, J.N., Wolff, L., Neau, E., Avaullee, L., 1998a. A very simple multiple mixing cell calculation to compute the minimum miscibility pressure whatever the displacement mechanism. Ind. Eng. Chem. Res. 37 (12), 4854-4859.

Jensen, F., Michelsen, M.L., 1990. Calculation of first contract and multiple contact minimum miscibility pressures. In Situ. 14 (1), 1-17.

Jhaveri, B.S., Youngren, G.K., 1988. Three-parameter modification of the Peng-Robinson equation of state to improve volumetric predictions. SPE Res. Eng. 3 (03), 1-033.

Johns, R.T., Dindoruk, B., Orr, F.M., 1993. Analytical theory of combined condensing/vaporizing gas drives. SPE Adv. Tech. Ser. 1 (02), 7-16.

Johns, R.T., Orr, F.M., 1996. Miscible gas displacement of multicomponent oils. SPE J. 1 (01), 39-50.

Johns, R.T., Sah, P., Solano, R., 2002. Effect of dispersion on local displacement efficiency for multicomponent enriched-gas floods above the minimum miscibility enrichment. SPE Res. Eval. Eng. 5 (01), 4-10.

Kantzas, A., Bryan, J., Taheri, S., 2012. Fundamentals of Fluid Flow in Porous Media.

Leibovici, C.F., Nichita, D.V., 2008. A new look at multiphase Rachford-Rice equations for negative flashes. Fluid Phase Equilibr. 267 (2), 127-132.

Li, H., Qin, J., Yang, D., 2012. An improved $CO_2$-oil minimum miscibility pressure correlation for live and dead crude oils. Ind. Eng. Chem. Res. 51 (8), 3516-3523.

Li, R., Li, H., 2019. A modified multiple-mixing-cell algorithm for minimum miscibility pressure prediction with the consideration of the asphaltene-precipitation effect. Ind. Eng. Chem. Res. 58 (33), 15332-15343.

Li, S., Li, Z., Dong, Q., 2016. Diffusion coefficients of supercritical $CO_2$ in oil-saturated cores under low permeability reservoir conditions. J. $CO_2$ Util. 14, 47-60.

Liu, K., Wu, Y., McHugh, M.A., Baled, H., Enick, R.M., Morreale, B.D., 2010. Equation of state modeling of high-pressure, high-temperature hydrocarbon density data. J. Supercrit. Fluid. 55 (2), 701-711.

Martin, J.J., 1979. Cubic equations of state-which? Ind. Eng. Chem. Fund. 18 (2), 81-97.

Mathias, P.M., Naheiri, T., Oh, E.M., 1989. A density correction for the Peng-Robinson equation of state. Fluid Phase Equilibr. 47 (1), 77-87.

Metcalfe, R.S., Fussell, D.D., Shelton, J.L., 1973. A multicell equilibrium separation model for the study of multiple contact miscibility in rich-gas drives. SPE J. 13 (03), 147-155.

Michelsen, M.L., 1982a. The isothermal flash problem. Part I. Stability. Fluid Phase Equilibr. 9 (1), 1-19.

Michelsen, M.L., 1982b. The isothermal flash problem. Part II. Phase-split calculation. Fluid Phase Equilibr. 9 (1), 21-40.

Monroe, W.W., Silva, M.K., Larson, L.L., Orr, F.M., 1990. Composition paths in four-component systems: effect of dissolved methane on 1D $CO_2$ flood performance. SPE Res. Eng. 5 (03), 423-432.

Orr, F.M., 2007. Theory of gas injection processes (Vol. 5). Copenhagen: Tie-Line Publications.

Orr, F.M., Johns, R.T., Dindoruk, B., 1993. Development of miscibility in four-component $CO_2$ floods. SPE Res. Eng. 8 (02), 135-142.

Pedersen, K.S., Christensen, P.L., Shaikh, J.A., 2014. Phase behavior of petroleum reservoir fluids. CRC press.

Péneloux, A., Rauzy, E., Fréze, R., 1982. A consistent correction for Redlich-Kwong-Soave volumes. Fluid Phase Equilibr. 8 (1), 7-23.

Peng, D.Y., Robinson, D.B., 1976. A new two-constant equation of state. Ind. Eng. Chem. Fund. 15 (1), 59-64.

Pitzer, K.S., 1955. The volumetric and thermodynamic properties of fluids. I. Theoretical basis and virial coefficients. J. Am. Chem. Soc. 77 (13), 3427-3433.

Qiu, Y., Chen, Y., Zhang, G.G., Yu, L., Mantri, R.V. eds., 2016. Developing solid oral dosage forms: pharmaceutical theory and practice. Academic press.

Rachford, H.H., Rice, J.D., 1952. Procedure to use electrical digital computers in calculating flash vaporization hydrocarbon equilibrium. AIME Pet. Trans. 195, 327-328.

Ratnakar, R.R., Dindoruk, B., Wilson, L., 2016a. Experimental investigation of DME-water-crude oil phase behavior and PVT modeling for the application of DME-enhanced water flooding. Fuel. 182, 188-197.

Ratnakar, R.R., Dindoruk, B., Wilson, L., 2016b. Use of DME as an EOR agent: experimental and modeling study to capture interactions of DME, brine and crudes at reservoir conditions. SPE 18515.

Ratnakar, R.R., Dindoruk, B., Wilson, L.C., 2017. Phase behavior experiments and PVT modeling of DME-brine-crude oil mixtures based on Huron-Vidal mixing rules for EOR applications. Fluid Phase Equilibr. 434, 49-62.

Robinson, D.B., Peng, D.Y., 1978. The characterization of the heptanes and heavier fractions. Reasearch Report. 28.

Robinson, D., Peng, D., Ng, H., 1979. Capabilities of the Peng-Robinson programs. 2. 3-phase and hydrate calculations. Hydro. Proc. 58 (9), 269-273.

Rowley, R.L., Wilding, W.V., Oscarson, J.L., 2007. DIPPR Project 801 data compilation of pure compound properties, AIChE DIPPR. New York.

Sebastian, H. M., Wenger, R. S., Renner, T.A., 1985. Correlation of minimum miscibility pressure for impure $CO_2$ streams. J. Pet. Technol. 37 (11), 2-076.

Shi, J., Li, H.A., 2016. Criterion for determining crossover phenomenon in volume-translated equation of states. Fluid Phase Equilibr. 430, 1-12.

Shi, J., Li, H.A., Pang, W., 2018. An improved volume translation strategy for PR EOS without crossover issue. Fluid Phase Equilibr. 470, 164-175.

Siregar, S., Mardisewojo, P., Kristanto, D., Tjahyadi, R., 1999. Dynamic interaction between $CO_2$ gas and crude oil in porous medium. SPE 57300.

Soave, G., 1972. Equilibrium constants from a modified Redlich-Kwong equation of state. Chem. Eng. Sci. 27 (6), 1197-1203.

Spencer, C.F., Danner, R.P., 1972. Improved equation for prediction of saturated liquid density. J. Chem. Eng. Data. 17 (2), 236-241.

Stalkup, F.I., 1983. Miscible Displacement (Vol. 8). NY: Society of Petroleum Engineers of AIME.

Standing, M.B., 1977. Volumetric and phase behavior of oil field hydrocarbon systems. Society of petroleum engineers of AIME.

Tallon, S., Fenton, K., 2010. The solubility of water in mixtures of dimethyl ether and carbon dioxide. Fluid Phase Equilibr. 298 (1), 60-66.

Tsang, C.Y., Streett, W.B., 1981. Vapor-liquid equilibrium in the system carbon dioxide/dimethyl ether. J. Chem. Eng. Data. 26 (2), 155-159.

van der Waals, J.D., 1873. Continuity of the gaseous and liquid state of matter. University of Leiden.

Wade, L.G., 2013. Organic chemistry: pearson new international edition. Pearson Higher Ed.

Wang, Y., Orr, F.M., 1997. Analytical calculation of minimum miscibility pressure. Fluid Phase Equilibr. 139 (1-2), 101-124.

Wang, Y., Orr, F.M., 2000. Calculation of minimum miscibility pressure. J. Petrol. Sci. Eng. 27 (3-4), 151-164.

Whitson, C.H., Brule, M.R., 2000. Phase Behavior (Vol. 20). SPE Monograph Series.

Whitson, C.H., Michelsen, M.L., 1989. The negative flash. Fluid Phase Equilibr. 53, 51-71.

Wilson, G.M., 1969, May. A modified Redlich-Kwong equation of state, application to general physical data calculations. In: 65th National AIChE Meeting, Cleveland, OH.

Yang, Z., Liu, X., Hua, Z., Ling, Y., Li, M., Lin, M., Dong, Z., 2015. Interfacial tension of $CO_2$ and crude oils under high pressure and temperature. Colloids Surf. A Physicochem. Eng. Asp. 482, 611-616.

Yellig, W.F., Metcalfe, R.S., 1980. Determination and prediction of $CO_2$ minimum miscibility pressures (includes associated paper 8876). J. Pet. Technol. 32 (01), 160-168.

Yuan, H., Johns, R.T., 2005. Simplified method for calculation of minimum miscibility pressure or enrichment. SPE J. 10 (04), 416-425.

Zick, A.A., 1986. A combined condensing/vaporizing mechanism in the displacement of oil by enriched gases. SPE 15493.